Influence of Tempering on the Microstructure & Properties of Martensite and Bainite developed in a Low-C High-Si Steel

Master student: Sihui Li

Project duration: November 2016 – September 2017

Thesis committee: Dr. M. J. Santofimia, TU Delft, supervisor & chair

Dr. B. Kim, TU Delft, supervisor

Dr. V. Popovich, TU Delft

Abstract

Martensitic and bainitic steels are two types of widely used steels with excellent mechanical behaviors in automatic industry. It's universally acknowledged that as-quenched martensite possesses poor ductility and impact toughness, which should be tempered before putting into application. During tempering, as-quenched martensite changes from a hard and brittle microstructure to more ductile and softer microstructure, leading to improved mechanical properties for manufacturing. Bainitic microstructures is less sensitive to tempering in the improvement of mechanical properties, while the explicit tempering effects are still unknown.

The primary goal of the current research is to study the effect of tempering on the microstructure and properties of martensitic and bainitic microstructures developed in the same low carbon steel with high content of silicon and manganese (0.2wt.%C-2wt.%Si-3wt.%Mn). Results show that for tempered martensite, the hardness, yield strength and tensile strength have a decreasing tendency with higher tempering temperatures. Through tempering, martensite became more ductile at the expense of strength. Based on the literatures, transitional carbide precipitation is expected to take place instead of cementite at early stage of tempering due to the retarding effect of high silicon content. Investigations also show that bainite is less sensitive to tempering compared to martensite. The yield strength and elongation firstly increase due to the TRIP effect of retained austenite and then decrease with higher tempering temperature. Hardness and tensile strength have a similar decreasing tendency as martensite during tempering. The fracture modes of tempered martensite for all temperatures show a typical ductile fracture, while for bainite, a morphology of quasi-cleavage fracture is observed.

Content

1 Introduction ……1

2 Literature Review……2
2.1 Martensitic and Bainitic Transformations..……2
2.1.1 Time-temperature-transformation Diagram…….2
2.1.2 Martensitic Transformations……3
2.1.3 Bainitic Transformations…….4
2.2 Martensitic and Bainitic Microstructures……..6
2.2.1 Martensitic Microstructures……6
2.2.2 Bainitic Microstructures……..8
2.3 Strengthening Mechanisms……...8
2.4 Tempering of Martensitic and Bainitic Microstructures…….11
2.4.1 Tempering of Martensitic Microstructures……11
2.4.2 Tempering of Bainitic Microstructures…….13
2.5 Research Objectives……..16
2.6 Structure of the Thesis……...16

3 Studied Material and Experimental Procedures……...17
3.1 Material of Study……...17
3.1.1 Chemical Composition and Microstructures ……17
3.1.2 Sample Size and Sample Preparation……17
3.2 Selection of Heat Treatment Parameters……...19
3.2.1 Continuous-cooling-transformation Curve and Calculation of Transformation Temperatures……..19
3.2.2 Heat Treatments……20
3.3 Tensile Test……..…23
3.4 Microstructure Characterization……..23
3.4.1 Optical Microscope……...23
3.4.2 Scanning Electron Microscope……..23
3.5 Hardness Test……...24

4 Results & Discussions……25
4.1 The Formation of Martensite and Bainite……...25
4.2 Tempering of Martensitic Microstructures……..27
4.2.1 As-quenched Martensite……..27
4.2.2 Effect of Tempering on Martensite…….28
4.3 Tempering of Bainitic Microstructures……...34
4.3.1 Bainitic Microstructures……..34
4.3.2 Effect of Tempering on Bainite……...36
4.4 Comparison of Martensite and Bainite during Tempering…….40

5 Conclusions……42
6 Recommendations……..44
References.....47

1 Introduction

In recent years, high strength steels have become a hot topic in the steelmaking industry. Two typical high strength steels, martensitic and bainitic steels have been widely used in the past decades.

The as-quenched state of martensitic microstructure possesses the highest strength and hardness which can be produced in a steel, and is not suitable for manufacturing and application. Therefore, tempering is performed as an efficient heat treatment method to modified the mechanical properties of martensitic microstructures [1] by choosing proper tempering parameters (tempering temperature and tempering time). Bainitic microstructure obtained through isothermal transformation is much tougher than as-quenched martensite [2].

Silicon is a critical alloyed element to inhibit the precipitation of cementite, leading to a more ductile steel. Silicon can control the tempering of martensite by inhibiting the cementite precipitation from supersaturated ferrite and austenite in a martensitic microstructure [3]. A sufficient quantity of silicon can also promote carbon partitioning into the residual austenite in a bainitic transformation, leading to a large quantity of retained austenite and some high-carbon martensite in the final bainitic microstructures [4]. Therefore, study the microstructural changes during tempering of martensitic and bainitic microstructures in a high silicon steel plays an important role.

2 Literature Review

In this chapter, key concepts related to the thesis are introduced, including the transformation and microstructure of martensite and bainite, strengthening mechanisms and also the tempering effects on both microstructures.

2.1 Martensitic and Bainitic Transformations

2.1.1 Time-temperature-transformation Diagram

In Fe-C alloys, austenite, with a face-centered cubic crystal structure, is the stable phase at high temperatures, in which carbon atoms occupy interstitial sites. When cooling the austenite at a certain rate, austenite will transform to other equilibrium phases at lower temperatures. The quantitative information of this transformation can be simply illustrated by a time-temperature-transformation diagram (TTT diagram) which consists of several roughly C-shaped curves, as shown in Figure 2.1 [2].

The three C-curves at higher temperature range represent diffusional transformation products such as pearlite in the original austenite grain. The curves from left to right represent that 1%, 50% and 95% of the transformation is completed, respectively. The curves at lower temperature range represent displacive reactions such as bainite and martensite. The resulting microstructures depend on both cooling rate and the temperature the material is cooled to. When a steel is cooled to a medium temperature, bainitic microstructures can be obtained which is shown by the curves lower than those of pearlite. With even fast cooling rate to room temperature, austenite directly transforms to martensite, the process of which is called martensitic transformation represented by the curves at the lowest positions [5, 6].

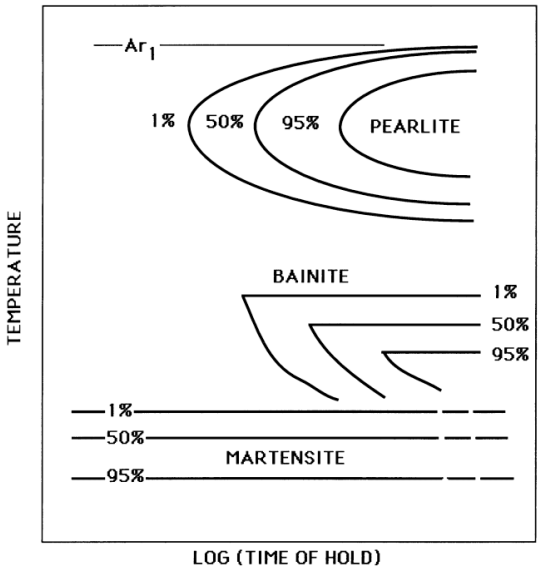

Figure 2.1: *Time-temperature-transformation diagram. Ar_1: the critical point at which ferrite transform completely into austenite during heating. Obtained from [2].*

2.1.2 Martensitic Transformations

Martensitic transformation is usually referred as a diffusionless transformation because it takes place through the lattice deformation of austenite without diffusion of carbon atoms. The fast cooling to room temperature leaves no time for the solid solution carbon atoms to diffuse out of the lattice of austenite, so the carbon atoms remain in solid solution in the new martensitic microstructure, as the original austenite [6]. When the temperature reaches the martensite-start transformation temperature M_s (the temperature at which austenite starts to transform to martensite) [7], austenite is no longer stabilized and starts to transform. The transformation ends at the martensite-finish temperature M_f which is usually defined as the point where 95% of the martensitic transformation is completed [6]. Austenite that remains untransformed is usually called retained austenite. Some related concepts in the martensitic transformation which will be mentioned in the following sections are briefly explained.

The habit plane

The habit plane refers to the broad interface plane between the austenite and martensite, as is illustrated in Figure 2.2. The interface is flat in unconstrained transformation, but curved during the constrained martensitic transformation to minimize the strain energy due to the deformation during the transformation. The curved planes lead to the thin plates or laths morphology of martensitic microstructures, which will be discussed later [6].

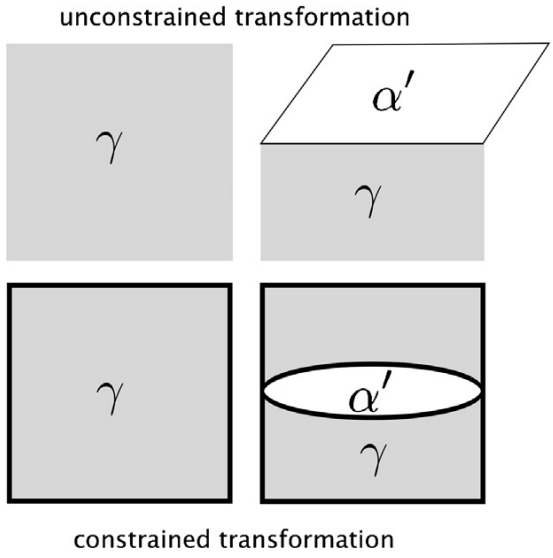

Figure 2.2: *An illustration of the habit plane between austenite (γ) and martensite (α′). Obtained from [6].*

Orientation relationships

During the transformation from austenite to martensite, carbon atoms experience coordinated movement inside the lattice, leading to some closely related relationships between the parent austenite lattice and the product martensite lattice. The most common orientation relationships in steels with low carbon contents is Kurd-jumov-Sachs (K-S) relationship where both the close-packed planes and close-packed directions are parallel in the two phases [8].

2.1.3 Bainitic Transformations

When austenite is cooled at a medium cooling rate to a temperature range of 250-550℃ and held for a certain time [2], a different microstructure, bainite, occurs and this process is called bainite formation.

Two alternative interpretations of bainite formation mechanism are acknowledged nowadays, namely diffusional and displacive interpretations. The diffusive interpretation states that the change in crystal structure (nucleation and growth of bainitic ferrite) during the transformation is mainly activated by diffusion-controlled movements of substitutional solutes in the austenite. The carbon concentration in the bainitic ferrite is equilibrium with that of the parent austenite. While the displacive interpretation sates that the bainitic transformation follows a diffusionless process similar to martensitic transformation. In this case, supersaturated bainitic ferrite with carbon forms displacively followed by carbon diffusing from ferrite into austenite or precipitating inside the ferrite as carbides [8, 9].

In the case of displacive reaction mechanism, carbon diffusion can occur and form precipitates between or within laths at different temperatures, leading to two typical microstructures, upper bainite and lower bainite, originally indicated by Mehl [10]. Figure 2.3 shows a scheme of the formation process of upper and lower bainite. The typical morphologies of upper and lower bainite under the optical microscope are shown in Figure 2.4.

Upper bainite

As is shown in Figure 2.3 for upper bainite, the nucleation of ferrite occurs in the austenite and the carbon diffuses into austenite. With decreasing temperature, the carbon follows a short range diffusion and segregates along the austenite boundary as carbide precipitates. The growth of ferrite also occurs inside the original austenite. Upper bainite, as is shown in Figure 2.4 (a), forms in the temperature range 500-400℃, showing fine ferrite plates of about 0.2 μm thick and 10 μm long each [6]. The typical morphology of upper bainite are parallel ferrite sheaves separated by untransformed austenite, martensite (α') or carbide precipitation, which is similar to that of martensite due to the same displacive transformation mechanism. Based on the definition of displacive transformation, bainite has a crystal structure which has an orientation relationship with the original austenite, usually described by a K-S type relationship which was introduced preciously. Under the optical microscopy, ferrite plates can be observed but no carbide precipitation between lath can be seen. Since ferrite usually nucleates along the austenite grain boundaries and grows in parallel direction inside the grains, upper bainite usually appears in a feathery morphology. The carbide precipitation between ferrite plates is generally considered to be cementite particles.

Lower bainite

In lower bainite, the ferrite is supersaturated with carbon and nucleates in carbon-depleted region. Due to the lower transformation temperature than upper bainite, the diffusion of carbon into austenite becomes more difficult and occur also inside the ferrite. Carbide precipitation occurs inside ferrite to minimize the free energy, accompanied by the growth of ferrite. Lower bainite, shown in Figure 2.4 (b), forms in the temperature range 400-250℃ in the bainite transformation. Lower bainite also consists of ferrite and carbide precipitation. The two-dimension morphology of lower bainite under optical microscopy is dark needle-like, which is similar to martensite lath and upper bainite. The major difference between lower and upper bainite is that carbide precipitation occurs inside the ferrite plates in lower bainite. The type of the carbide depends largely on the transformation temperature and chemical composition of the steel [6-8, 11].

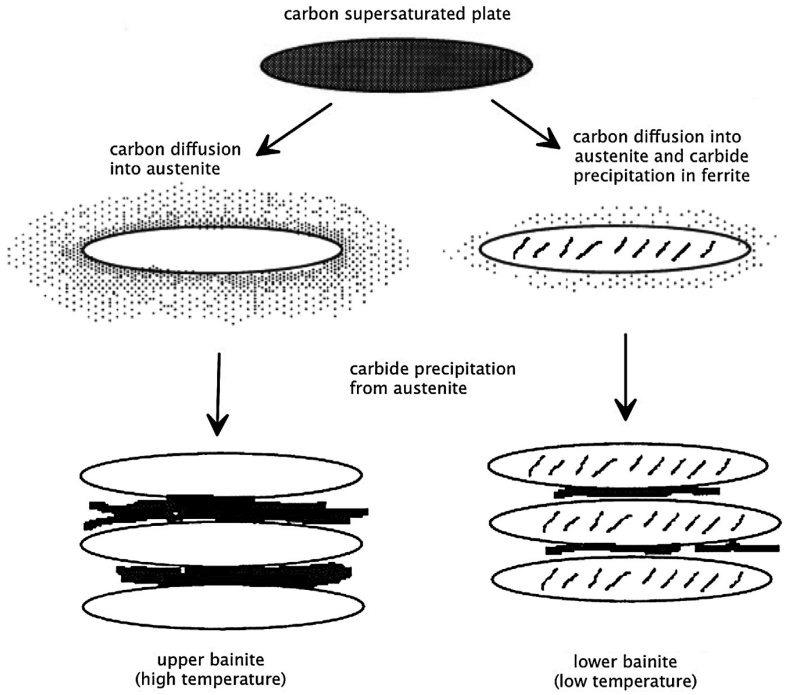

Figure 2.3: *Schematic representation of upper and lower bainite. Obtained from [6].*

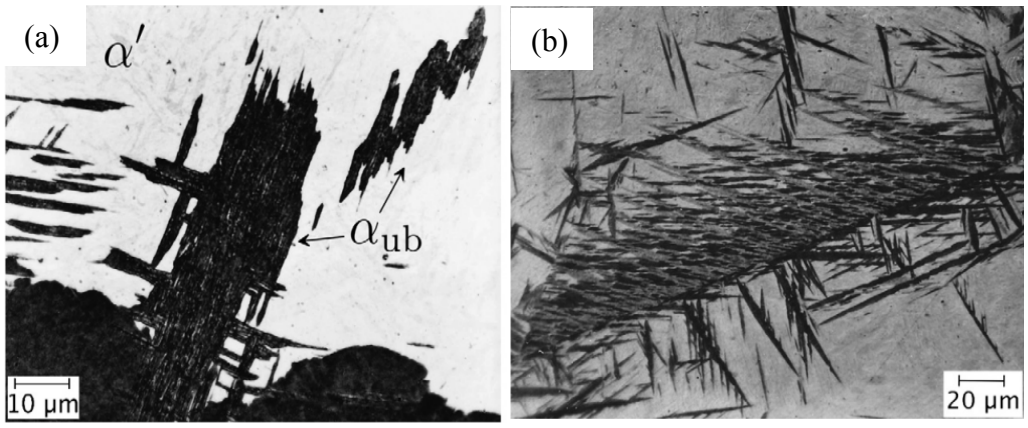

Figure 2.4: *Optical micrographs of (a) upper bainite (α_{ub}) and martensite (α') in Fe-0.8C wt.% steel, transformed 20 s at 400℃ and (b) lower bainite sheaves in Fe-0.8C wt.% steel transformed at 300℃. Obtained from [6].*

2.2 Martensitic and Bainitic Microstructures

2.2.1 Martensitic Microstructures

Figure 2.5 shows the optical micrographs of two typical morphologies of martensite, lath and plate martensite. Figure 2.6 shows the substructure for lath martensite in a low carbon steel [13].

Lath martensite is observed in low alloyed steels with carbon content less than 0.4 wt.% [14]. Lath martensite tend to align themselves to one another in the parent austenite grain, showing groups of parallel laths at an optical microscopic scale with a typical width of approximately 0.5 μm [8]. The sub structures of lath martensite, schematically illustrated in Figure 2.6 for a low carbon alloy, are quite complicated due to the sudden and independent growth of laths until the sub structures reach the former austenite grain boundaries. Researches show that in one single parent austenite grain, there are packets representing groups of laths with the same habit plane. And in one single packet, there are blocks representing groups of laths of the same orientation [13]. The size of these complicated sub-microstructures also plays an important role in determining the strength and toughness of lath martensite, which will be discussed later in this chapter [14].

Plate or lenticular (in three dimensions) martensite gets its name from its mutually inclined plates morphology, which usually occurs in medium and high carbon steels with carbon content higher than 0.4%. When the carbon content reaches 0.8%, plate martensite itself determines the microstructure [8,13]. The studied steel in this project contains 0.2%C and lath morphology is likely to occur.

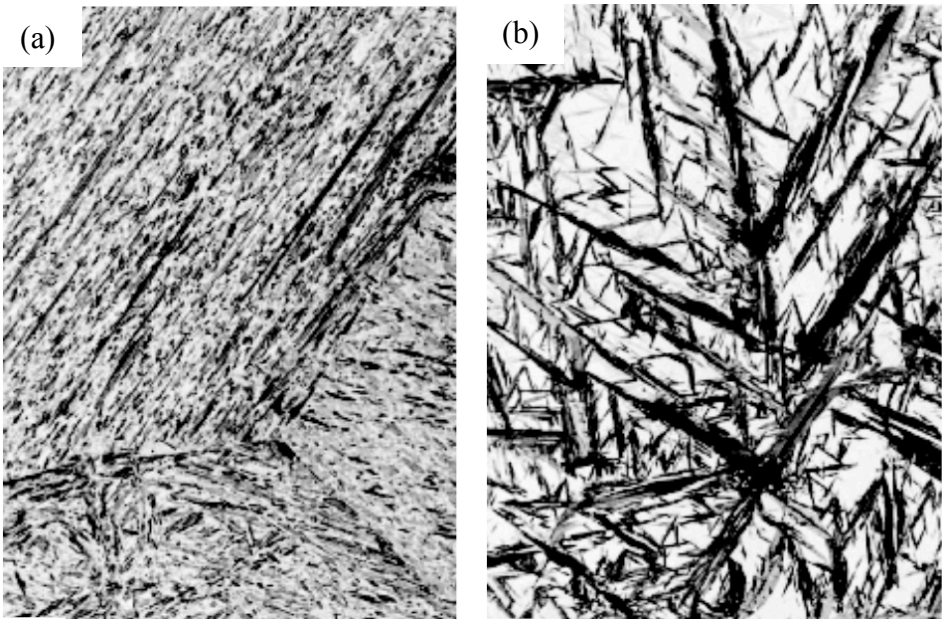

Figure 2.5: *Martensitic microstructures (low optical micrograph) (a) lath martensite (low-alloy steel with 0.17 wt.%C, 1200°C hot bath) (b) plate martensite (case-hardening steel, 1100°C hot bath). Obtained from [15].*

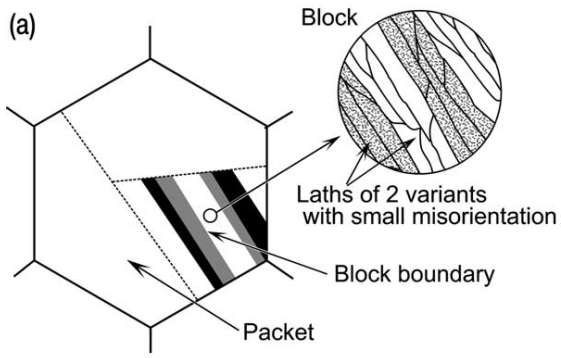

Figure 2.6: *Schematic illustrations showing lath martensite substructure in a low carbon alloy (0-0.4%C). Obtained from [13].*

2.2.2 Bainitic Microstructures

Since typical bainitic microstructures have already been introduced in the previous section, this section mainly focuses on the bainitic microstructure formed by isothermal treatment in a steel with high silicon content.

Silicon has the effect of retarding carbide precipitation in bainite formation. If sufficient quantities of silicon (around 1.5wt.%Si [9]) are added into the steel, it is possible to obtain a carbide-free constituent and a large quantity of carbon-enriched retained austenite during the isothermal transformation. The retained austenite is mainly located as the thin films in bainitic ferrite laths and MA blocks (M-fresh martensite, A-retained austenite). These MA blocks form during the final quenching to room temperature when austenite partially transforms to fresh martensite at grain boundaries. Tempered martensite formed during the austempering process is also expected in the final [16, 17]. Figure 2.7 shows a typical the bainitic microstructure of a steel with chemical composition of Fe-0.3C-1.5Si (wt.%), austempering at 380℃, in the form of a Kikuchi Pattern Quality map [17].

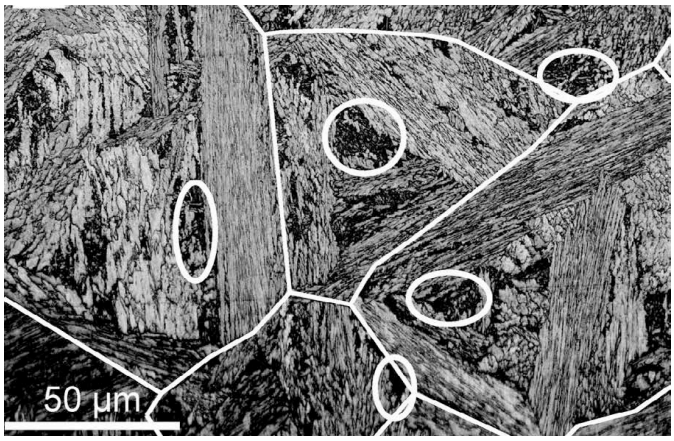

Figure 2.7: *Kikuchi Pattern Quality map of a low carbon high silicon steel (Fe-0.3C-1.5Si, wt.%) elaborated at austempering temperature at 380℃. The parent austenite grain boundaries are highlighted by white lines and MA blocks are indicated in white circles. Obtained from [17].*

Retained austenite provides the main contribution to the plasticity of the steel. Generally, bainite has excellent ductility due to the present of retained austenite between ferrite laths. It can slow the initiation and propagation of cracks and contributes with the TRIP effect. It also presents highly coherent interfaces with low interfacial energy, which has negative effect on the propagation of cracks [18].

2.3 Strengthening Mechanisms

Tempering influences the microstructures of bainite and martensite, leading to changes in mechanical properties, especially in strength. The relationship between microstructure and strength can be understood by strengthening mechanisms in steels, which are shared by both martensite and bainite. For the most typical lath martensite and bainite, the strength mainly comes from the following aspects: strain hardening, solid solution strengthening, precipitation hardening and grain boundary hardening [19].

Dislocation strengthening

Dislocation strengthening, alternatively referred to as work hardening, strengthens the material during plastic deformation. Strain hardening, firstly interpreted by G.I. Taylor in 1934 [20], results from the dislocation interaction. During straining, the dislocation density in the microstructure greatly increases, leading to more intense interaction between dislocations and hindering the dislocation movement. Also, large amount of mobile dislocations are introduced during the phase transformations, contributing greatly to the strength of the microstructures. A universal stress provide by dislocation, σ_ρ , can be simply calculated by the Taylor equation [21] (Equation 2.1), which is proportional to the square root of the dislocation density,

$$\sigma_\rho = \alpha M G b \sqrt{\rho} \tag{2.1}$$

where α is a geometrical constant between 0.3 and 0.6, M is the Taylor factor, G is the shear modulus, b is the burgers vector of the dislocation and ρ is the dislocation density.

Solid solution strengthening

Solid solution hardening of carbon atoms is considered to make the most contribution to the macroscopic strength through the interaction with dislocations. The solid solute atoms are added into the matrix and cause lattice distortion due to the size difference, hindering the motion of dislocations and increasing the strength the steel. The solid solution strengthening of individual phases results from the contribution of interstitial carbon atoms and substituted alloying elements in the steel. The overall strength contributed by solid solutes, σ_{ss}, can be described by Equation 2.2. The strength

resulted from carbon atoms, σ_c , and substitutional atoms, σ_{st}, can be universally calculated by Equation 2.3 and 2.4, respectively.

$$\sigma_{ss} = \sigma_c + \sigma_{st} \tag{2.2}$$

$$\sigma_c = 1720(X_c)^{1/2} \tag{2.3}$$

$$\sigma_{st} = 83X_{Si} + 32X_{Mn} - 31X_{Cr} + 39X_{Cu} \tag{2.4}$$

where X_c (wt.%) represents the concentration of solid solute carbon in martensite and bainite, and X_j represent the concentration of alloying element j (j =Si, Mn, Cr and Cu). This equation has been applied for steels with alloying element concentration in the range of 4-5 wt.% [22].

Precipitation strengthening by carbides

When secondary particles form discrete precipitates, they can act as obstacles to dislocation movement following complicated mechanisms. There are two fundamentally form of particles interacting with dislocations, cutting and passing-by mechanisms, as is shown in Figure 2.8 [19, 23].

In the case of (a), when a dislocation encounters strong impenetrable particles, their interaction follows Orowan mechanism [24]. The dislocation line bends when confronting two particles separated by a distance of λ and gradually reaches a critical curvature during the movement. When the segments of dislocation meet each other on the opposite direction, the stress on the two dislocation segments cancel out, leaving a dislocation loop around the particles. Then the dislocation line is free to move along its original direction. The yield stress determined by this passing mechanism is inversely proportional to the distances between particles, which is expressed in Equation 2.5.

$$\sigma_{pass} = Gb/\lambda \tag{2.5}$$

When the particles are coherent with the dislocations, illustrated in (b), dislocations can shear the particles and move on. Equation 2.6 describes the misfit stress provided by the cutting mechanism,

$$\sigma_{cut} \propto G\varepsilon^{\frac{3}{2}}(rf)^{\frac{1}{2}} \tag{2.6}$$

where ε is misfit strain which is proportional to lattice parameter mismatch, r is the particle radius and f is the volume of a particle [23, 24].

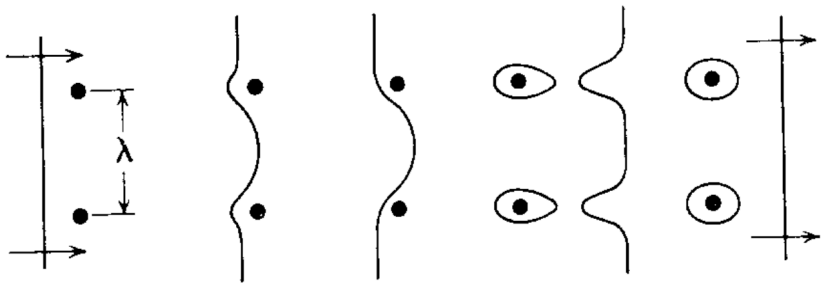

(a) A dislocation passing by two particles.

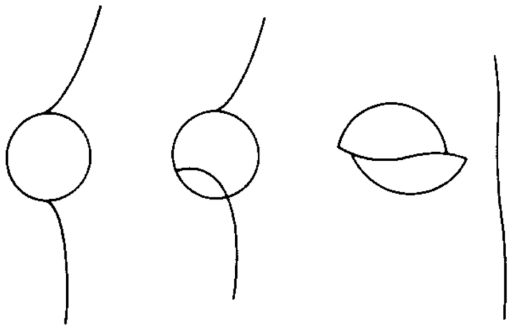

(b) A dislocation cutting a particle.

Figure 2.8: *Schematic drawing of two mechanisms of dislocation interacted with particles. Black dots represent particles and the line represents dislocation line. The arrow points to the direction of dislocation motion. Obtained from [23].*

Grain boundary strengthening

Grain boundaries usually act the obstacles to dislocation motion due to the different orientations between two crystals. Grain boundary strengthening, also called grain refining, is a process during which the grain size is reduced and the total area of grain boundaries are enhanced, causing difficult dislocation slip. The strength comes from the dislocation pile-up and the exist of block boundaries which hinder the slip of dislocations. The grain boundary strengthening of the constituent phases are determined by the Hall-Petch equation as follows [21],

$$\sigma_{gb} = \frac{K_{HP}}{\sqrt{d_{gb}}} \tag{2.7}$$

where d_{gb} represents the effective grain size of martensite or bainite. K_{HP} is a constant, named Hall-Petch slope.

Transformation-induced-plasticity (TRIP) effect refers to a phase transformation driven by plastic deformation from retained austenite phases to martensite phase, making it hard to deform in a local position. The necking is proponed and the ductility is enhanced during the phase transformation. The strength is also improved by the increased dislocation density during plastic deformation via the dilation of retained austenite [6, 8]. TRIP effect is strongly affected by the volume fraction and the stability of retained austenite, which is mainly determined by the carbon content in the austenite phase, the morphology, grain size and the position (the distribution of surrounding phases of retained austenite).

2.4 Tempering of Martensitic and Bainitic Microstructures

In this section, tempering effects from literatures on martensitic and bainitic microstructures will be introduced separately.

2.4.1 Tempering of Martensitic Microstructures

The as-quenched state of martensite is heavily dislocated after the martensitic transformation. The dislocation density of martensite for a 0.2 wt.% carbon steel can reach as high as 1.0×10^{18} m^{-2} [6]. Therefore, most of the steels are required to go through a further tempering process after martensic transformation. Tempering is an efficient way to eliminate the internal residual stress caused by the quenching process through carbide precipitation and enhance the mechanical properties.

Tempering of martensite is classified into four independent and overlapped stage based on tempering temperatures. With higher tempering temperatures, hardness decreases during stages of tempering of martensitic steel, as shown in Figure 2.9 [6]. This tendency will be explained later with the explicit microstructural changes during tempering.

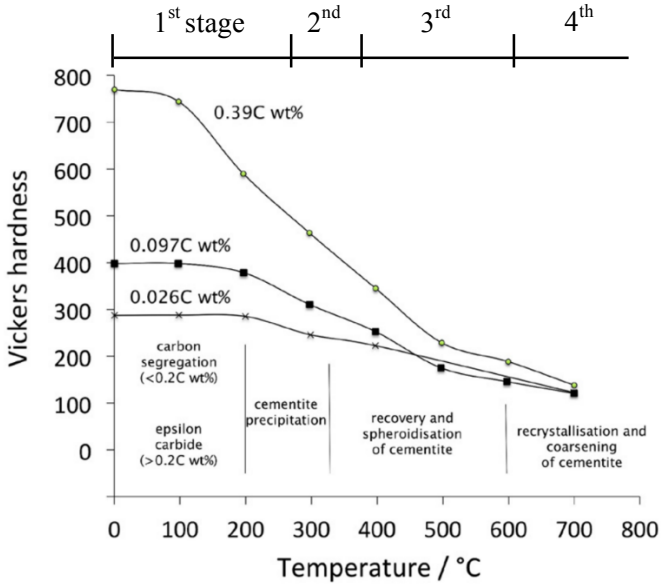

Figure 2.9: *Hardness of iron-carbon martensite tempered 1 h at 100-700℃. Obtained from [6]. Stage 1-4 represent the tempering states, but are overlapped in temperatures.*

1st stage of tempering

With temperature rises from room temperature to around 250℃, martensite becomes increasingly unstable due to the diffusion of interstitial carbon atoms. At this temperature range, transition carbides start to precipitate in the martensite, leading to precipitation hardening in the martensite. For steels with carbon content lower than 0.2%, carbides are not likely to precipitate and carbon segregation occurs.

2nd stage of tempering

With higher temperature, the austenite retained from quenching begin to decompose to bainitic ferrite and cementite. Generally, the change in austenite fraction is difficult to reveal directly due to its low concentration in the as-quenched microstructure. In silicon-rich steels, the formation of cementite at this stage is retarded and cannot be observed in this temperature range. Silicon can stabilize ε-carbide, leading to the increase of the decomposition temperature.

3rd stage of tempering

During this stage, cementite starts to nucleate at ε-iron carbide interfaces with the matrix. As the cementite grows, the unstable ε-carbide particles are gradually replaced by cementite, which may occur from 100℃ to 300℃. Another energetic favorable nucleation site for cementite is the grain boundaries (both martensite and parent austenite), along which the cementite particles tend to coarse and be spherodized with higher temperature. The hardness begins to drop slightly with the precipitation of cementite.

4th stage of tempering

During the 4th stage, cementite gets coarser and spheroidization occurs. The coarsening process starts between 300℃ and 400℃ while the spheroidization lasts until 700℃. At this high temperature, martensite laths are replaced by large amount of equiaxial ferrite grain boundaries and the whole process is described as recrystallization. The final microstructure after tempering contains new ferrite grains and Fe_3C particles on the grain boundaries. Before temperature reaching 600℃, the lath boundaries of martensite remain stable. In the temperature range between 350 to 600℃, large amount of dislocations realigns inside and along the lath boundaries, leading to a significant decrease in dislocation density and forming lath-like ferrite. This process is called recovery [6,8,13].

The hardness for steels with different carbon concentration generally decreases with increasing tempering temperature. During the tempering process, the carbon in solid solution precipitates into carbides and then coarse cementite, significantly eliminating the solid solution strengthening of carbon. In the last two stages of tempering, recovery and recrystallization occur, accompanying by a significant decrease in dislocation density, which leads to drop of hardness. In addition, higher carbon concentration leads

to higher hardness because more carbon is in the solid solution, contributing strongly to strength and hardness [6].

2.4.2 Tempering of Bainitic Microstructures

The effect of tempering on bainitic microstructure is not as strong as that of martensite, the main reason being that the ferrite in bainite is less supersaturated in carbon [8]. Tempering is a process during which solid solute carbon become carbide precipitation, yet for both upper and lower bainite, there already existing cementite and other carbides in the microstructures. Figure 2.10 shows a relation curve between the hardness and the tempering parameter for two bainitc steels. It can be indicated that the carbon concentration does not influence much on the hardness of bainite during tempering, which confirms that in bainitic microstructures, the carbon is not in solid solution but in the form of carbide precipitates, which contribute little to the strength of the steel [2]. In addition, the quantities of hardness drop during tempering of bainite is much less than that during tempering of martensite.

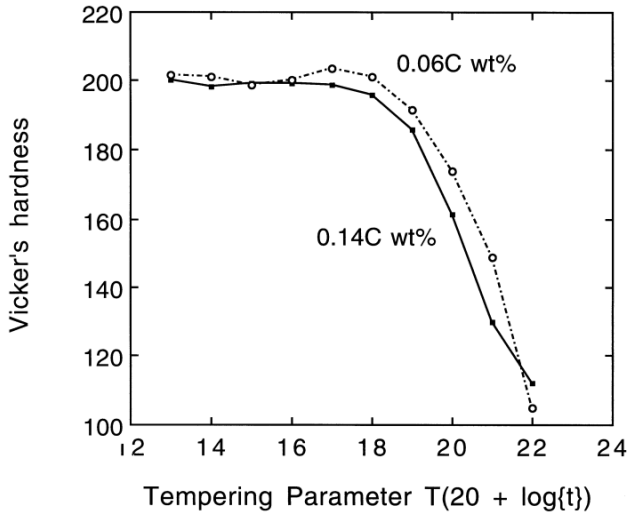

Figure 2.10: *Change in hardness for two bainitic steels with different carbon contents as a function of tempering parameter. Obtained from [2].*

Decomposition of retained austenite

In silicon-rich bainitic steels, as mentioned previously, large quantity of carbon-enriched austenite is retained in MA blocks and as thin films among the bainitic sheaves [2]. In tempering of bainite, block-like austenite tends to primarily decompose to ferrite and cementite because the retained austenite films are more stable due to the higher carbon content than in the block [25]. With silicon retarding the formation of cementite, only transition carbides precipitation is expected in a silicon-rich steel. Kang et al. [26] studied the tempering effect of bainite developed in a steel (Fe-0.46C-1.55Si, wt.%), the microstructures of which are shown in Figure 2.11. The tempered bainitic sheaves

show needle-like morphology. In the TEM picture, it can be observed that bainitic ferrite is separated by retained austenite films. Blocks cannot be observed, which confirms the primary decomposition of block-like austenite. Tempering at 450℃, bainitic ferrite significant coarsens and fine carbides are observed, resulting from the decomposition of thin-film retained austenite and the precipitation inside the bianitic ferrite plates. In addition, with higher tempering temperature, the dislocation density evidently drops, indicating the recovery and recrystallization at high temperatures during tempering.

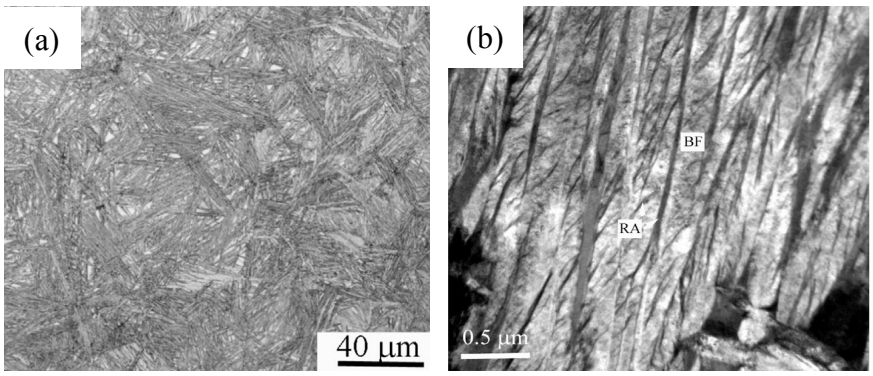

Figure 2.11: *(a) OM microstructures and (b) TEM microstructures of a medium carbon high silicon steel (Fe-0.46C-1.55Si), isothermal transformed at 270*℃ *followed by tempering at 240*℃*. RA-retained austenite. BF-bainitic ferrite. Obtained from [26].*

Precipitation of cementite

The aim of precipitation and coarsening of cementite is to minimize the stored energy in the interfaces, which occur in the tempering process of martensite and bainite. In lower bainite, cementite particles are in two forms: finely dispersed inside the laths and precipitated at the lath boundaries. For upper bainite, cementite only occurs at the lath boundaries. Figure 2.12 shows the change of cementite size during tempering at 700 ℃ in a medium carbon high silicon steel (Fe-0.45C-0.22Si-0.62Mn wt.%) [2]. The upper and lower shaded regions represent the cementite on the lath boundaries in martensite and within the laths in lower bainite, respectively. It can be observed that the coarsening rate of martensite during tempering is much faster than that of bainite. This is because during tempering, large amount of cementite precipitation occurs in martensite within laths and on the boundaries, resulting in a large total number density of particles. The bainitic microstructure is more stable during tempering, with relatively finer cementite even after long tempering time.

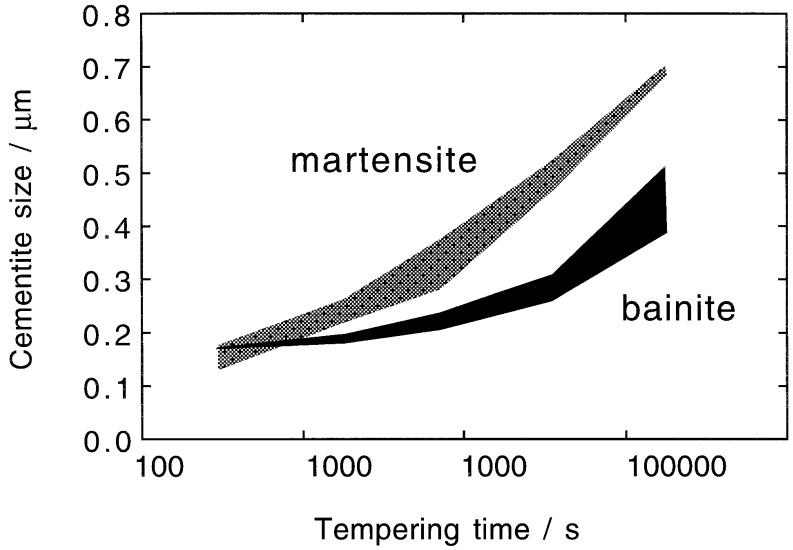

Figure 2.12: *Coarsening of cementite during the tempering of a medium carbon steel. Bainite is isothermally formed at 380*℃*. Obtained from [2].*

2.5 Research Objectives

Tempering is thought to be a most effective heat treatment to improve the mechanical properties of as-quenched martensite. Compared to martensite, bainitic microstructures, with less carbon in solid solution in ferrite, are thought to be less sensitive to tempering under the same conditions. By adding silicon as an alloyed element in steels, cementite precipitation during tempering and bainitic transformation will be suppressed, leading to different tempering effects on the microstructure and properties of both martensite and bainite in the silicon rich steel.

This thesis therefore aims to investigate how tempering process with different tempering temperatures and times influence the microstructure and mechanical behaviors of martensite and bainite developed in a low carbon steel with high silicon and high manganese content. Similarities and differences between martensite and bainite through tempering will also be studied. In addition, fractography of tensile fracture will be discussed preliminary.

2.6 Structure of the Thesis

The rest of the thesis containing following chapters:
Chapter 3 presents the experimental contents, including studied materials, experimental procedures and applied techniques.
Chapter 4 presents the results and discussion of the project.
Chapter 5 presents the conclusion and recommendations of the project.

3 Studied Material and Experimental Procedures

3.1 Material of study

The studied material in this project is a hot-rolled steel received as a steel sheet with thickness of 6 mm. The rolling process was done in four passes in the temperature range of 1100-885℃. Chemical composition of the steel and sample preparation before are introduced in this section.

3.1.1 Chemical Composition and Microstructure

The studied material is a low carbon steel with chemical composition illustrated in Table 3.1. The studied material is a steel with carbon concentration of 0.2C with 1.97Si and 2.93Mn (wt.%) as two major alloyed elements.

***Table 3.1**: Chemical composition of the studied material.*

Element	C	Mn	Si	Cr	P	S	Al	N
Content(wt.%)	0.2	2.93	1.97	<0.05	<0.002	<0.001	0.009	<0.001

Figure 3.1 shows the microstructure of the studied material under two different magnifications cutting from a blank of 6-mm thick. During dendritic solidification, the substitutional alloying elements segregate and form regions with different Mn concentrations, leading to banded microstructure along the rolling direction after hot rolling, which is shown in Figure 3.1 (a). Light-etched region and dark lath morphology can be observed in (b), illustrating a mixed microstructure of ferrite and martensite.

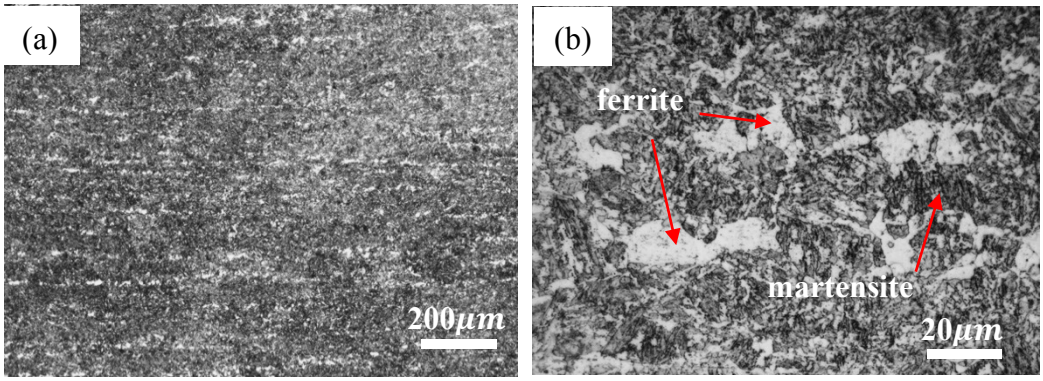

***Figure 3.1:** Optical microscopy image of the as-received material. (a) Banded microstructure. (b) Mixed microstructure of ferrite and martensite which are indicated by arrows. 2% Nital etched.*

3.1.2Sample Size and Sample Preparation

The material was received as a steel slab with 120 mm and thickness of 6 mm, and is cut into 14 blanks with 120 mm × 15 mm × 6 mm, shown in Figure 3.2 (a-b), perpendicular to rolling direction based on the 14 different heat treatment conditions decided in this research. Each blank went through the heat treatment separately and machined. Due to the original size of the as-received material, two subsize ASTM tensile test specimens were manufactured from one blank, the size information of which is illustrated in Figure 3.2 (c). In total, 28 subsize tensile test specimens were prepared for the experiments afterwards [27].

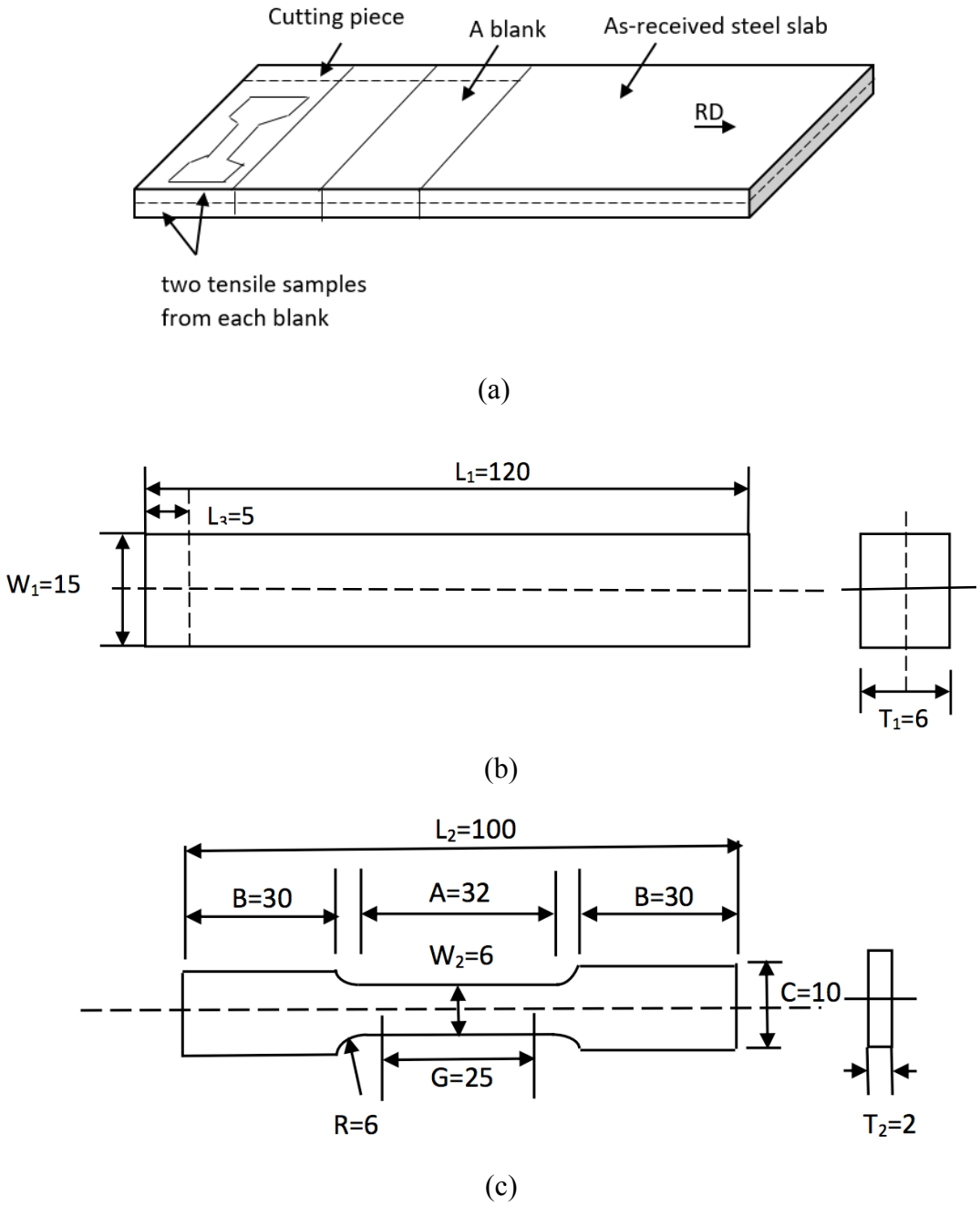

Figure 3.2: *The scheme of (a) material preparation process (b) blank from the steel sheet (c) subsize tensile test specimen from one blank (mm). G-Gage length; W_1-Width*

of a blank; W_2-Width of a specimen; T_1-Thickness of a blank; T_2-Thickness of a specimen; R-Radius of fillet; L_1-Overall length of a blank; L_2-Overall length of a specimen; L_3-length of the cutting part; A-Length of reduced section; B-Length of grip section. C-Width of grip section. Size information are obtained from [27].

After the heat treatment, one piece of the steel of about 5 mm length (shown in Figure 3.2 (a)) was cut from one end of each blank, which was used to perform further optical and scanning electron microscope observations and afterwards, hardness testing.

The samples were firstly grinded with sandpapers from P180 to P2000, then polished to 1 μ, presenting a mirror-like surface without any scratches under optical microscope. After polishing, the surfaces of the samples were etched with 2% Nital solution to reveal the microstructures of the surface.

3.2 Selection of Heat Treatment Parameters

This section includes the selection methodology of heat treatment parameters, i.e. how to obtain martensitic and bainitic microstructure and how to determine the tempering temperatures and times.

3.2.1 Continuous-cooling-transformation Curve and Calculation of Transformation Temperatures

In order to obtain martensitic and bainitic microstructure before tempering, a CCT curve of the studied steel was firstly calculated using JMatPro, which is illustrated in Figure 3.3. In the CCT diagram, dashed lines represent different cooling rates from 100.0℃/s to 0.1℃/s, falling in the regions of different microstructures. The lines consisting of colored dots represent the start (0.1% of the transformation is completed) and finish (99.9% of the transformation is completed) boundaries of different transformation products, with increasing temperature process.

With the fastest cooling of 100.0℃/s to room temperature, i.e. quenching, within 10s, martensitic microstructures are expected to occur, the principle of which was discussed in Chapter 2.

With cooling rate of 10.0℃/s, the cooling line firstly reaches a bainite-start temperature (referred to B_s temperature) at around 450℃, where bainite starts to form. Eventually the line falls into the region separated by the bainitic-start and bainitic-finish temperature boundaries, representing the formation of bainitic microstructure at this cooling rate.

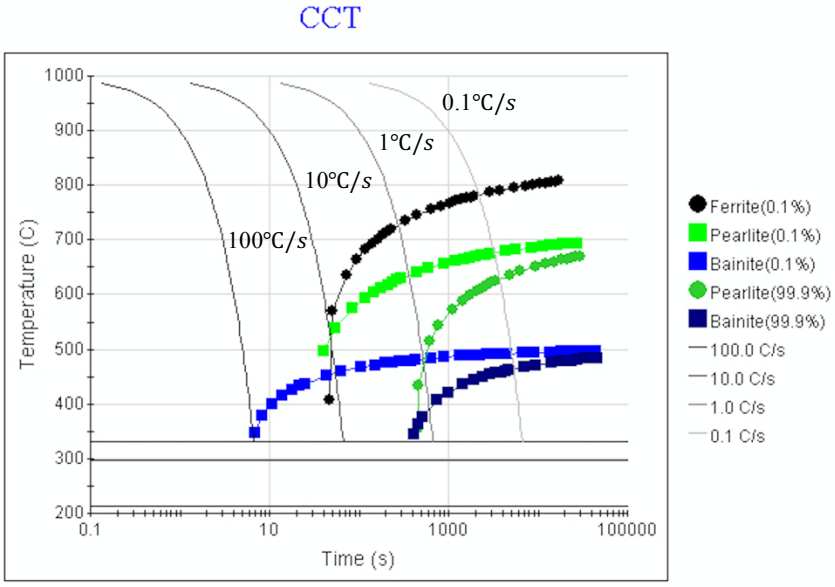

Figure 3.3: *The CCT curve of the studied steel.*

To select the heat treatment parameters, the transformation temperatures (A_{c1}, A_{c3}, M_s and B_s temperatures) are also calculated using empirical equations as follows from Eq. (3.1) to Eq. (3.4) [28-31].

$$A_{c1}(℃) = 723 - 16.9(wt.\%Ni) + 29.1(wt.\%Si) + 6.38(wt.\%W) - 10.7(wt.\%Mn) + 16.9(wt.\%Cr) + 290(wt.\%As) = 749.1℃ \quad (3.1)$$

$$A_{c3}(℃) = 955 - 350(wt.\%C) + 25(wt.\%Mn) + 51(wt.\%Si) - 106(wt.\%Nb) + 100(wt.\%Ti) + 68(wt.\%Al) - 11(wt.\%Cr) - 33(wt.\%Ni) - 16(wt.\%Cu) + 67(wt.\%Mo) = 921.0℃ \quad (3.2)$$

$$M_s(℃) = 462 - 273(wt.\%C) - 26(wt.\%Mn) - 16(wt.\%Ni) - 13(wt.\%Cr) - 30(wt.\%Mo) = 329.4℃ \quad (3.3)$$

$$B_s(℃) = 656 - 57.7(wt.\%C) - 75(wt.\%Si) - 35(wt.\%Mn) - 15.3(wt.\%Ni) - 34(wt.\%Cr) - 41.2(wt.\%Mo) = 389.5℃ \quad (3.4)$$

3.2.2 Heat Treatments

Based on the CCT curve and calculated transformation temperatures, the heat treatments in this project are determined and schematically illustrated in Figure 3.4 for martensitic microstructures and Figure 3.5 for bainitic microstructures.

Martensitic microstructures

Figure 3.4 shows the heat treatments performed for martensitic microstructures. The samples are firstly austenized in a Snustaal Nabertherm boxfurnace at 1000℃ for 5 min, followed by water quench to room temperature (25℃) to obtain as-quenched martensite. Then the samples were dried in a Venticell furnace of 75℃ for around 15min (shortest time for the samples to be completely dried) to avoid bringing water into further salt bath which would lead to eruption. Finally, the tempering treatments were performed in Snijstaal and Degussa salt bath at varied tempering temperatures 250, 400 and 500℃. 0.5 and 1 h tempering were performed for each temperature. The tempering treatments were followed by a final quenching in water to room temperature. In this paper, the martensitic samples tempered at 250℃ for 0.5 h and 1 h were represented as M250℃-0.5h and M250℃-1h. The same nomination principles were applied for tempering of 400 and 500℃, i.e. M400℃-0.5h, M400℃-1h, M500℃-0.5h and M500℃-1h.

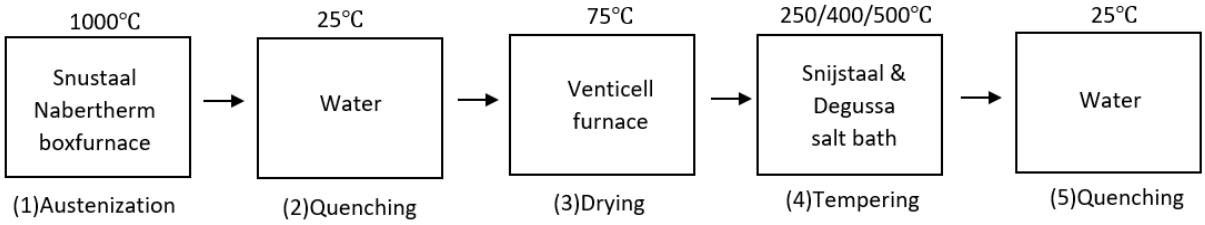

(a) Scheme of the heat treatment steps and the applied equipment.

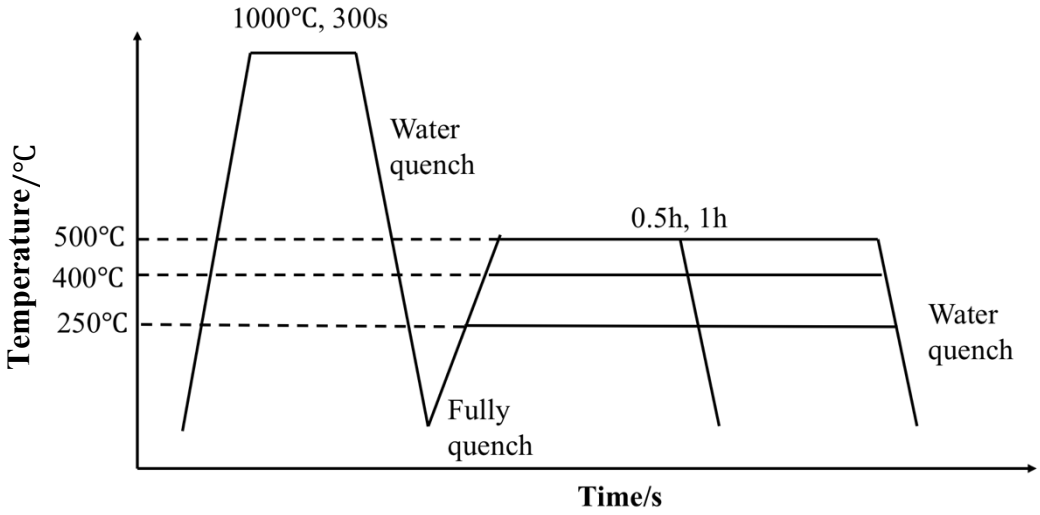

(a) Heat treatment graph for martensitic microstructures.

Figure 3.4: *Schematic representation of heat treatment performed for martensitic microstructures.*

Bainitic microstructures

Figure 3.5 shows the heat treatments performed for bainitic microstructures. The samples were austenized at 1000℃ for 5 min and then transferred to a Snijstaal salt bath at 400℃ for 30min. These isothermal treatments were followed by water quench to room temperature. Then the samples were drying in a Venticell furnace at 75℃ for around 15 min. Finally, the tempering treatments were performed in Snijstaal and Degussa salt bath at varied tempering temperatures 250, 400 and 500℃. 0.5 and 1 h tempering were performed for each temperature, similar to martensite. The tempering treatments were followed by a final quenching in water to room temperature. In this paper, the bainitic samples tempered at 250℃ for 0.5 h and 1 h were represented as B250℃-0.5h and B250℃-1h. The same nomination principles were applied for tempering of 400 and 500℃, i.e. B400℃-0.5h, B400℃-1h, B500℃-0.5h and B500℃-1h.

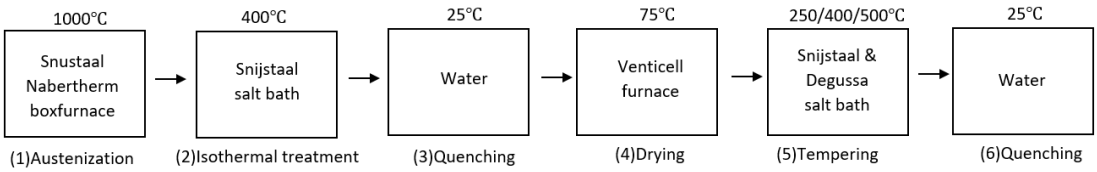

(a) Scheme of the heat treatment steps and the applied equipment.

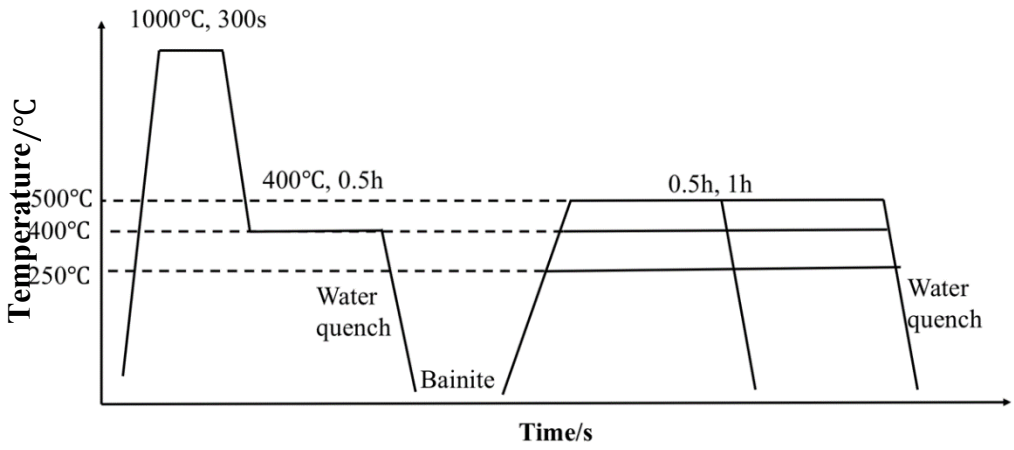

(b) Heat treatment graph for bainitic microstructures.

Figure 3.5: *Schematic representation of heat treatment performed for bainitic microstructures.*

The pictures of equipment mentioned above are illustrated in Figure 3.6. A pair of thermocouples were attached at the center of the blank to record the temperature and time profile during the heating and quenching process, which will be presented in Chapter 4. They were removed after the first quenching of both martensite and bainite.

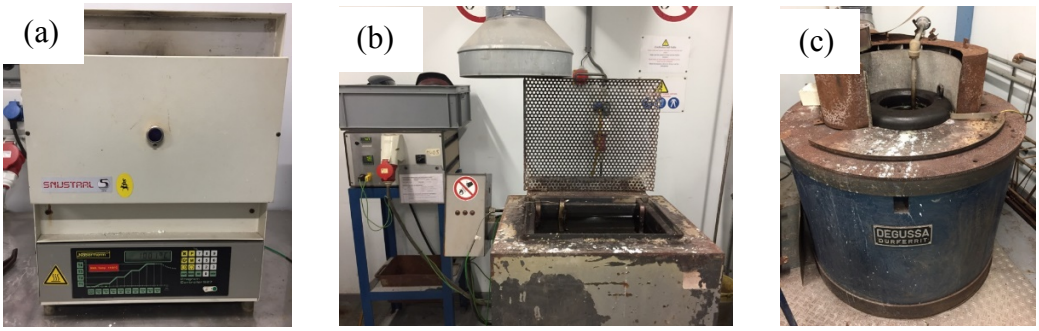

Figure 3.6: *Box furnace and salt bath used in the heat treatment process. (a) Snustaal Nabertherm Boxfurnace (b) Snijstaal salt bath (c) Degussa salt bath.*

3.3 Tensile Test

Oxidation layers were removed by sand papers of P320 and P800 before tensile testing. Tensile testing was performed at a constant strain rate of 2 mm/s on a Instron 55EOR tensile machine. The gauge length of tensile specimens was 25 mm. Figure 3.7 shows a tensile specimen under tensile testing.

Figure 3.7: *A tensile specimen during necking.*

3.4 Microstructure Characterization

3.4.1 Optical Microscope

Optical microscope is a widely used technique to observe the surface microstructure of samples in the lab. After etching, micro constituents with different chemical potential react differently with Nital and reveal as dark and bright region. In this way, different microstructure can be observed [27, 32]. Olympus BX60M microscope is used in this project.

3.4.2 Scanning Electron Microscope

When there is limitation in the magnification of the optical microscope, scanning electron microscope is used to observe the morphology in more detailed [32]. In this project, JSM-IT100 manufacturing by JEOL is used to reveal the microstructural change during tempering. The precipitation of carbide and the change of volume fraction of phases can be roughly characterized under SEM.

The observation of the fracture surfaces after tensile testing of the samples was performed using SEM to reveal the fracture type and its link to the mechanical behaviors of the samples. Figure 3.8 shows the way of fractography observation.

Figure 3.8: *Sketch of the way of fractography observation using SEM.*

3.5 Hardness Test

Vickers hardness of each sample was tested using a Vickers hardness test machine, DuraScan70. An indenter is forced into the material surface with a static load, leaving an impression on the surface, the size of which is measured by a microscope. The most accurate hardness values are obtained from an application load (kg) that give an impression with a diagonal length of about 0.5 mm [33]. Pre-experiment trials were performed and the 1kg indenter (referred to as HV1) was chosen. 10 points were tested in each sample in one row to increase the accuracy of the results. The hardness value for each sample was represented in the form of the average value with standard deviation value of the HV1 calculated from the 10 impressions.

4 Results & Discussions

The results of microstructure and mechanical behaviors obtained from the experiments are shown and discussed in this chapter. Tempering effects of martensite and bainite are explained separately, including the microstructural changes during tempering process and the related mechanical behaviors. Fractography results are also discussed for both microstructures.

4.1 The Formation of Martensite and Bainite

Figure 4.1 illustrates the cooling profiles recorded by the thermocouples during the austenization and quenching process of M250℃-0.5h and B500℃-0.5h samples. The heating and cooling rates (r) concerned are calculated by Equation 4.1 as follows:

$$r = \left| \frac{T_2 - T_1}{t_2 - t_1} \right| \tag{4.1}$$

where T_2 and T_1 represent the finish and start temperatures, t_2 and t_1 represent the finish and start times, reading from the graphs. The cooling rate of each quenching process can be obtained from the enlarged graph.

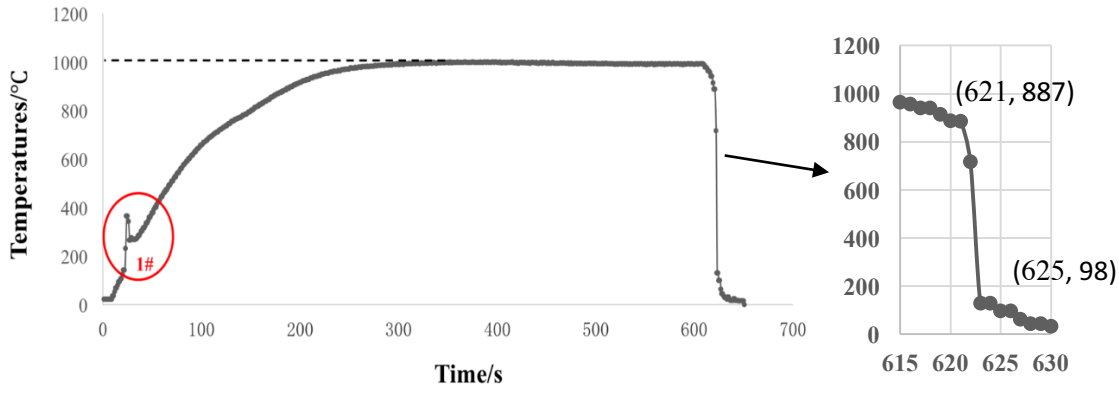

(a) Cooling profile of M250℃-0.5h. Cooling rate ~200℃/s.

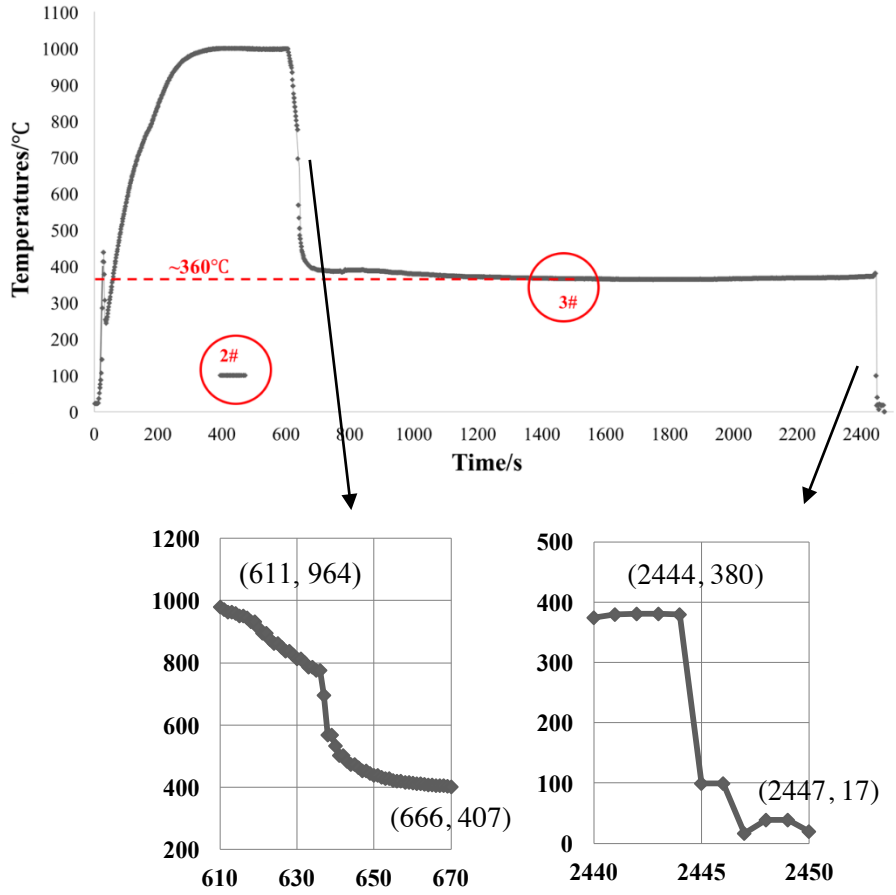

(b) Cooling profile of B500℃*-0.5h. Cooling rate of first and final cooling~10*℃*/s* and *120*℃*/s, respectively.*

Figure 4.1: *Temperature-time profiles for (a) martensite and (b) bainite.*

All samples went through the same austenization process with heating rate of approximately 3℃/s. For martensitic transformation, the quenching rate was about 200℃/s, much faster than the cooling rate boundary value 100℃/s in the previous CCT curve, indicating that austenite transformed directly to martensitic microstructures. For bainitic transformation, the rate of the 1st cooling was approximately 10℃/s to 400℃, which was coincide with the values in CCT curve, resulting in bainitic microstructures. The 2nd cooling rate of bainite after the isothermal treatment to room temperature was 120℃/s. According to the CCT curve, austenite to martensite transformation may occur.

Some deviations were observed in the temperature-time profile. As shown in the red circle 1# in Figure 4.1 (a), an increasing and dropping temperature range between 200℃ to 400℃ took place in almost all the specimen profiles. This unstable temperature change was caused by the cold atmosphere which entered the high temperature furnace when putting the sample in, leading to a temperature fluctuation in the furnace. After a short heating, the profile became normal and continuous. The red circle 2# in (b) shows

some points back to 100℃ causing by the unstable attachment of the thermocouples at that time. Red circle 3# illustrates a slightly deviation in isothermal temperature, from the theoretical value of 400℃ to around 360℃ in the experiments. This phenomenon was also caused by the unstable connection between the thermocouples and the salt bath, which can be considered as a machine error.

4.2 Tempering of Martensitic Microstructures

4.2.1 As-quenched Martensite

Microstructure characterization

The optical microscopy image (a) and SEM image (b) of as-quenched martensite are illustrated in Figure 4.2.

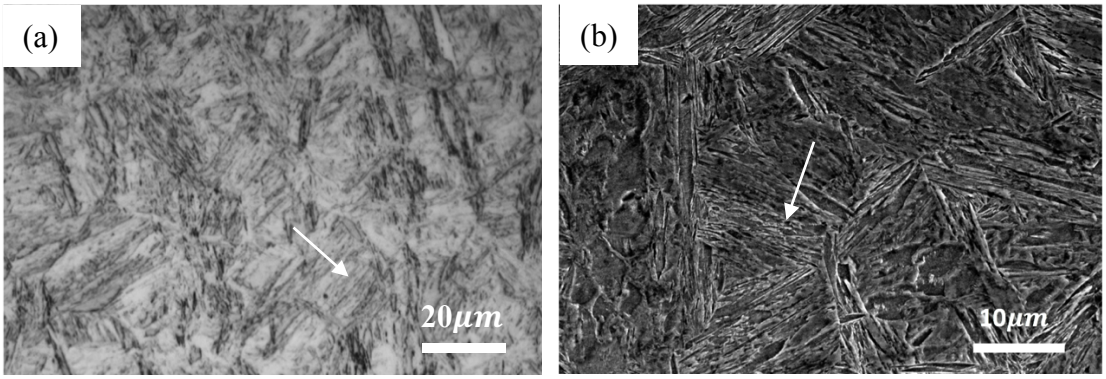

Figure 4.2: *As-quenched martensite austenized at 1000*℃ *and water quenched, showing lath morphology. (a) Optical micrograph (b) SEM micrograph. 2% Nital etched. White arrows show lath-like morphology.*

According to XRD results by Hu [34] for the same steel, the volume fraction of retained austenite in the fully-quenched specimen is approximately 1% and the volume fraction of martensite is approximately 99%. Clear lath-like martensite can be clearly observed from the image indicated by the arrows in (a) and (b). A single lath is around 10 μm long and 1-2μm wide. Retained austenite is hardly observed under optical microscope and SEM due to its low volume fraction and similar lath-like morphology as martensite. Due to the diffusionless transformation during quenching, the chemical composition of martensite is the same as parent austenite. Compared to the as-received material, the lath martensite distribute more homogeneously in the microstructure.

Mechanical properties

The mechanical properties of as-quenched martensite are shown in Table 4.1.

Table 4.1: *Mechanical properties of as-quenched martensite.*

	Hardness/HV1	YS/MPa	UTS/MPa	Elong./%
Martensite	521 ± 9	1205 ± 16	1663 ± 4	8.0 ± 0.1

During fast cooling, large amount of dislocations was formed in the martensite, together with the solid solution strengthening resulted from carbon, leading to a brittle and hard microstructure.

Fractography

Figure 4.3 shows the SEM images of different magnifications of the fracture surface after tensile tests of as-quenched martensite.

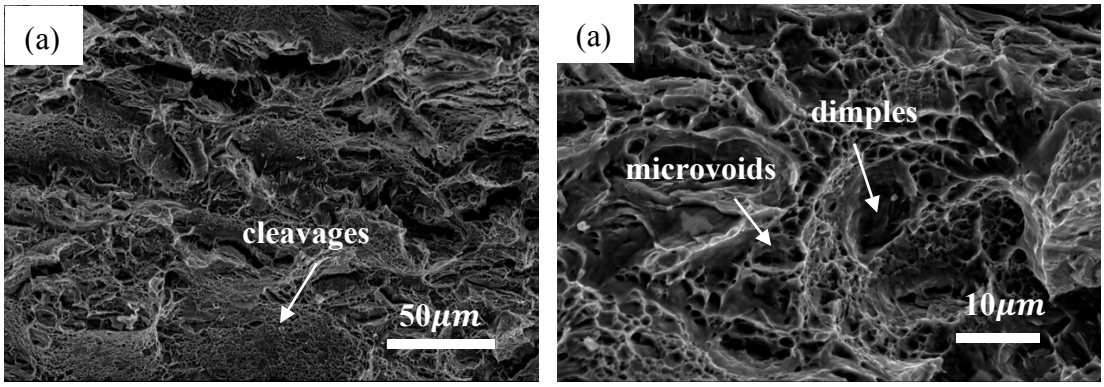

Figure 4.3: *SEM images of martensite before tempering.*

In Figure 4.3 (a), it can be observed that the microstructure is occupied by dimples and cleavages. Ductile dimples and microvoids, shown by white arrows in (b) with larger magnification are observed, indicating a ductile fracture mode. Also, some cleavage planes with atomic steps are also seen, indicated by the arrows in (a), representing the brittle fracture mode. As a hard and brittle phase, the fracture mode of the as-quenched martensite is a mixture of ductile and brittle fracture.

4.2.2 Effect of Tempering on Martensite

Microstructure characterization

Figure 4.4 (a-f) shows the optical microscope micrographs of martensitic microstructures after tempering. Figure 4.5 (a-d) shows the SEM micrographs of martensitic microstructures after tempering.

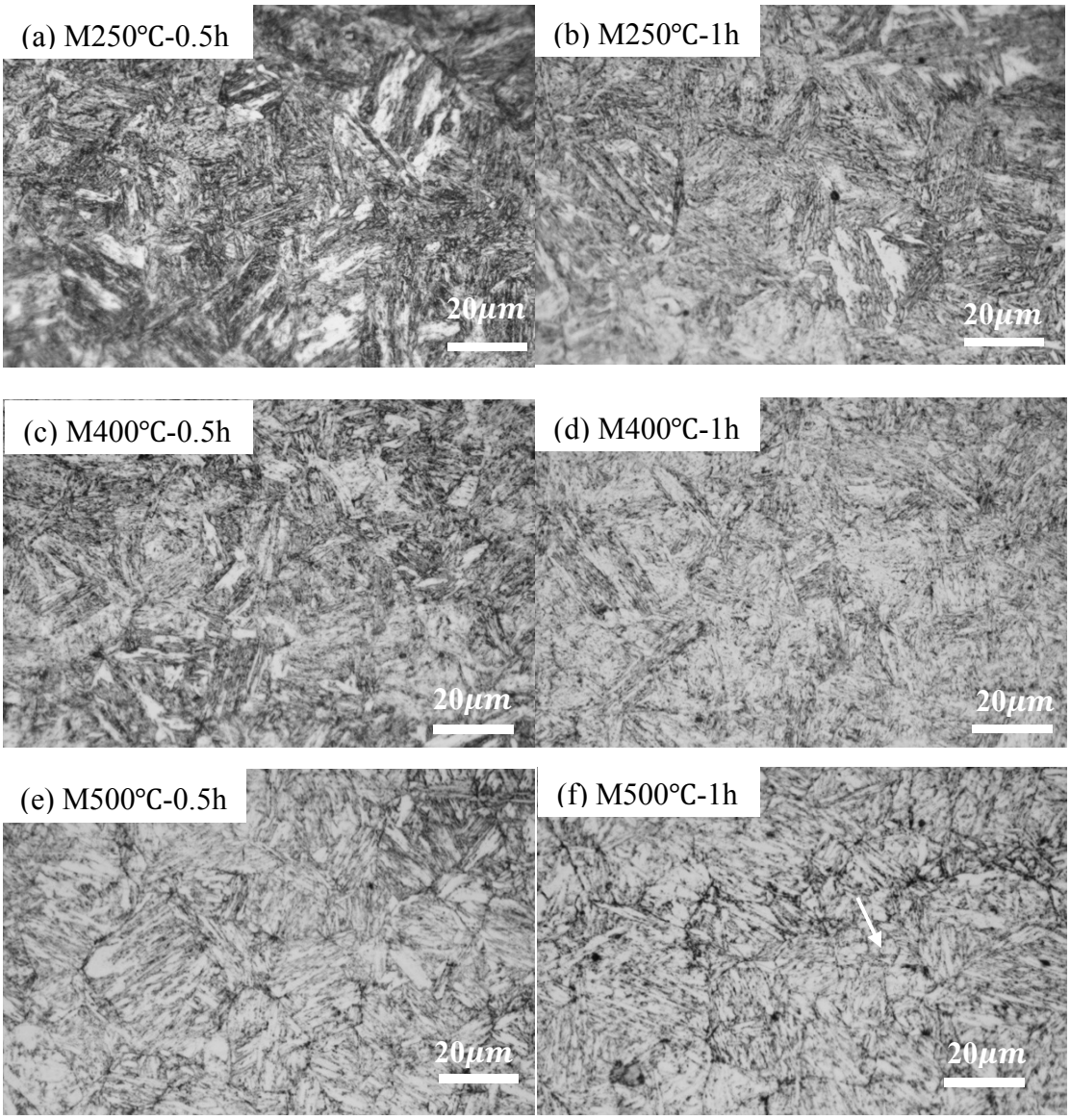

Figure 4.4: *Optical images of tempered martensite of different tempering temperatures and times from (a-f). 2% Nital etched.*

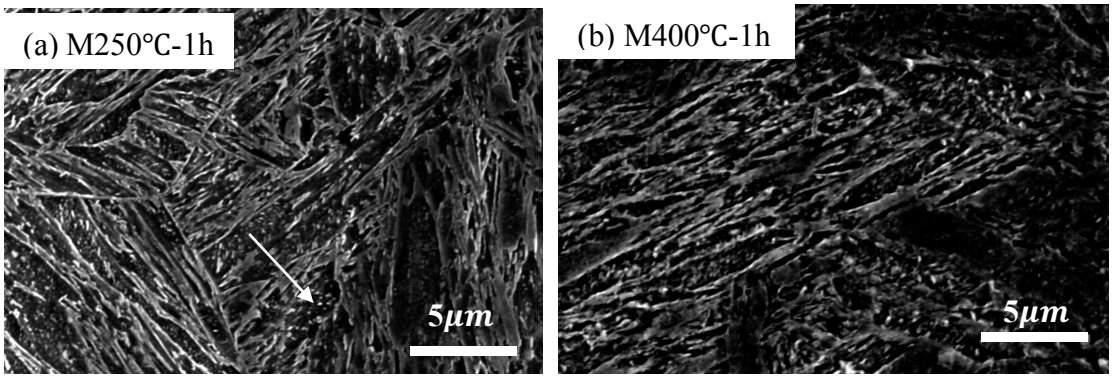

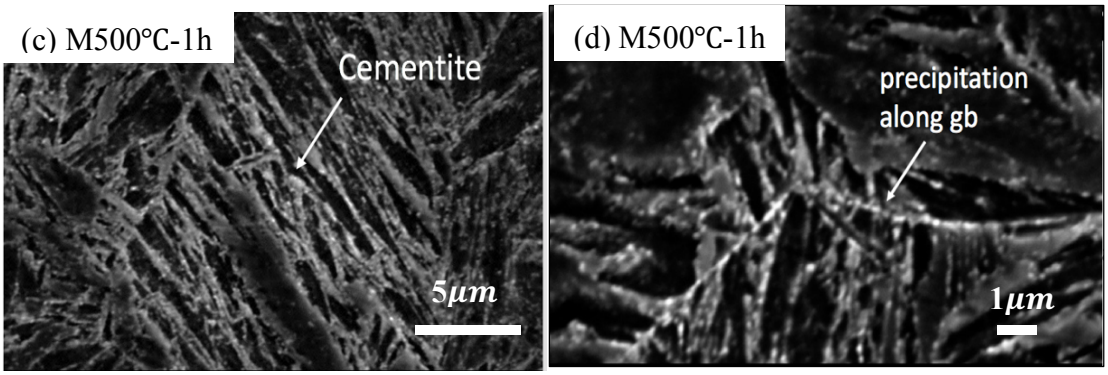

Figure 4.5: *SEM images of tempered martensite of different tempering temperatures for 1h from (a-d). 2% Nital etched.*

For samples of all three tempering temperatures, no obvious differences can be revealed in the microstructures for tempering time of 0.5h and 1h under the optical microscopy. Similar lath-like morphology is observed for both tempering times.

From Figure 4.4 (a-b) and Figure 4.5 (a), fine lath morphology separated by clear grain boundaries is observed for martensite tempered at 250℃, for 0.5h and 1h. Certain carbide precipitation occur inside the ferrite, indicated by arrows in Figure 4.5 (a). Due to the retarding effect of alloyed silicon in the steel, these precipitates are considered to be ε-carbide precipitating from super-saturated ferrite during tempering instead of cementite at this temperature.

For tempering temperature at 400℃, the lath-like morphology is reserved, as observed in Figure 4.4 (c-d) and Figure 4.5 (b). The size of martensite lath doesn't change much. Slightly coarser carbide precipitation can be observed, but the amount of carbide precipitation is quite similar to that of 250℃ inside the ferrite.

For tempering temperature at 500℃, the garin boundaries become clearer. Bright particles (represented by arrows in Figure 4.5 (c-d)) indicate the formation of more carbide particles along the boundaries of martensite lath and the prior austenite grain boundaries. In addition, more homogenous lath-like microstructure is observed due to the recrystallization of ferrite. Small amount of equiaxed array of ferrite grains and coarse spheroidized cementite particles can be observed in Figure 4.4 (f), indicating that some recovery and recrystallization occur at tempering temperature of 500℃.

Mechanical Properties

The mechanical properties of as-quenched and tempered martensite were characterized by hardness and tensile tests. The results are displayed in Table 4.2. The influence of tempering treatments on yield strength, ultimate tensile strength, total elongation and room temperature hardness with varying tempering temperature and times were plotted in Figure 4.6 (a)-(d).

Table 4.2: *Mechanical properties of tempered martensite.*

Sample	Hardness/HV1	YS/MPa	UTS/MPa	Elong./%
M250°C-0.5h	471 ± 8	1216 ± 13	1524 ± 10	7.7 ± 0.8
M250°C-1h	477 ± 8	1224 ± 1	1517 ± 1	8.0 ± 0.4
M400°C-0.5h	451 ± 5	1222 ± 18	1411 ± 15	8.9 ± 0.1
M400°C-1h	456 ± 10	1212 ± 9	1401 ± 13	8.2 ± 0.6
M500°C-0.5h	357 ± 3	1003 ± 3	1088 ± 2	11 ± 0.1
M500°C-1h	350 ± 7	975 ± 4	1067 ± 5	11.5 ± 0.6

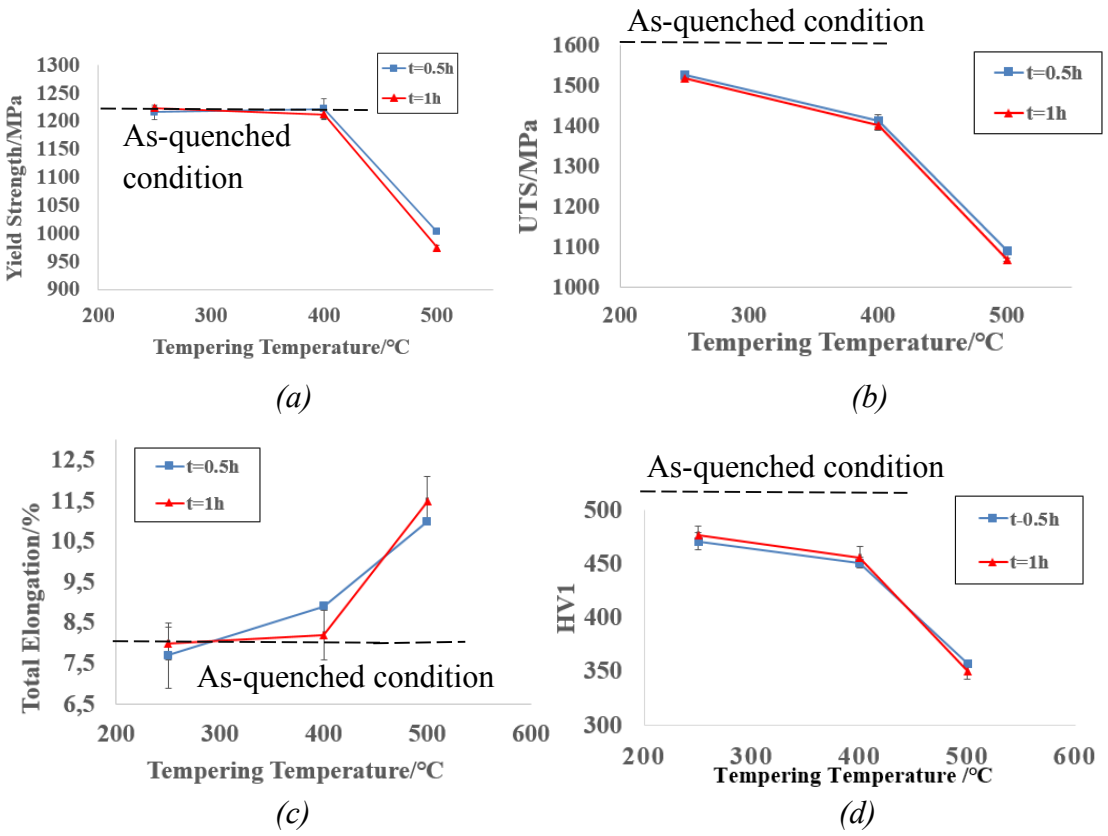

Figure 4.6: *Results of mechanical tests with increasing tempering temperatures. The dashed line in each figure indicates the mechanical properties of as-quenched martensite.*

From Table 4.2 and Figure 4.6, mechanical properties have changed with the increasing tempering temperature. Overall, the yield-tensile ratio is relatively high, which corresponds to the very few retained austenite (1%) in the microstructure. Higher tempering temperature enhanced the kinetics of dislocation movement, relieves the residual stress and makes the pile-up dislocation mobile again, leading to a decrease in strength and hardness.

The yield strength remains almost the in specimens tempered at temperatures up to 400℃. On one hand, dislocation density decreases due to recovery, leading to a softening effect of the matrix. On the other hand, the carbon precipitate from the martensite, increasing the strength of the matrix by precipitation strengthening. These two effects compensated each other and the yield strength remains the same.

When the tempering temperature increases to 500℃, the precipitates grow and the precipitation strengthening effect decreases. The yield strength decreases significantly due to the recovery of dislocations. Different from the tendency of yield strength, the ultimate tensile strength of martensite decreases continuously with increasing tempering temperature. This difference is because the tensile strength can only be influenced by the recovered dislocations in the ferrite matrix. Although large amount of carbide precipitates from martensite during tempering, it doesn't have much influence on the tensile strength. The hardness usually follows the same tendency with tensile strength in the tempering of steels, which also decreases continuously with increasing tempering temperature.

The total elongation of tempered martensite increases with the increasing tempering temperature. With increasing temperature, dislocation density decreases and recovery and recrystallization occur in the ferrite matrix, causing the increasing of ductility.

Fractography

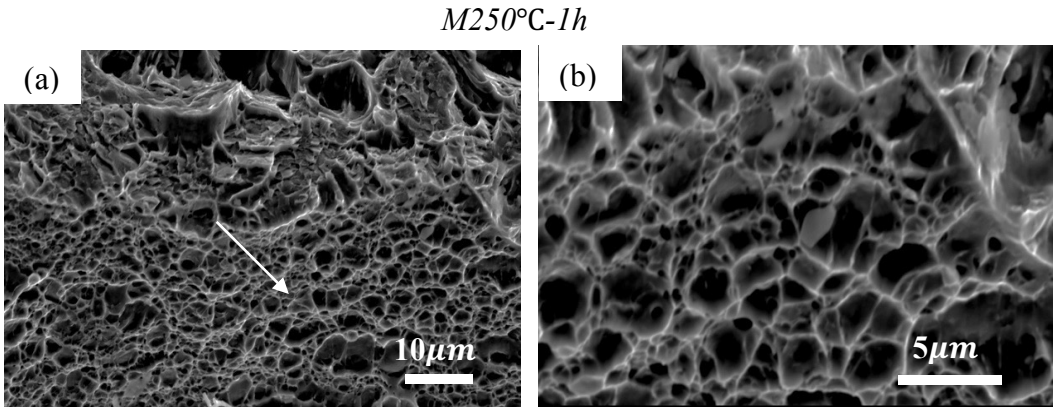

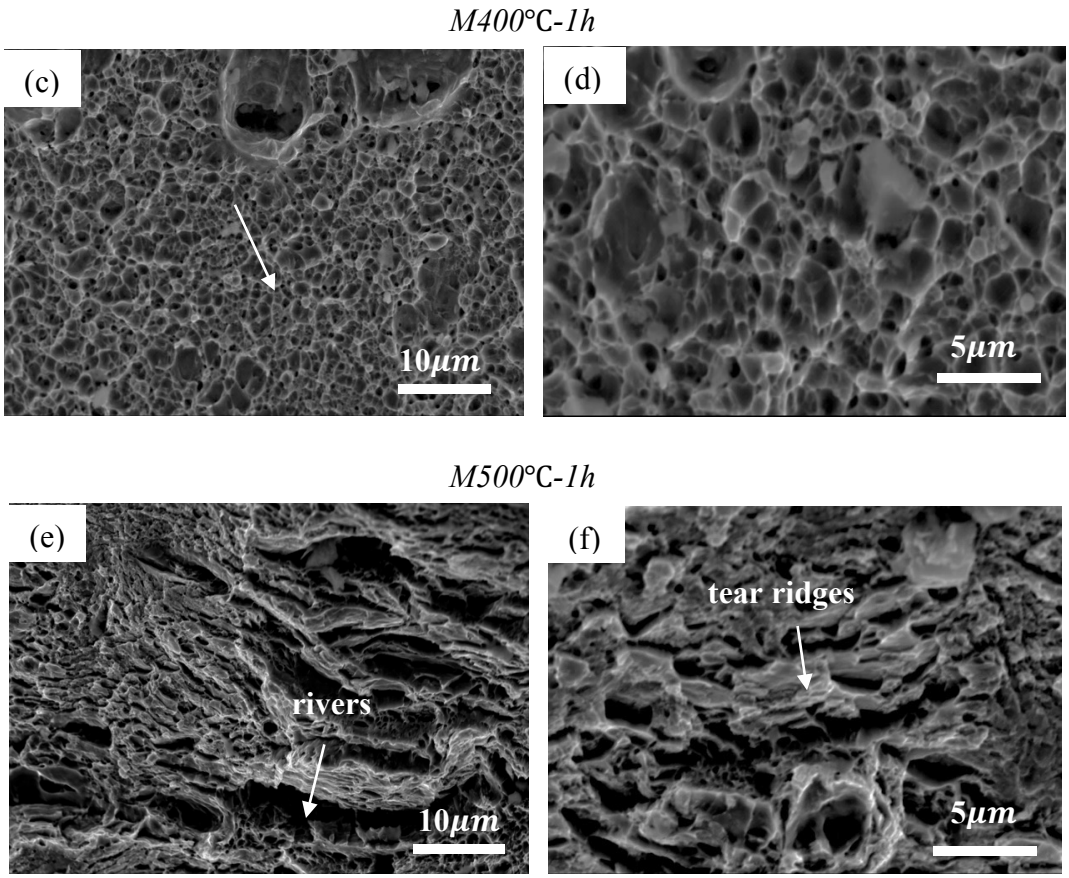

Figure 4.7: *SEM micrographs of the fracture surface of tempered martensite after tensile tests with tempering temperature of 1h.*

Figure 4.7 illustrates the fracture surfaces of tempered martensite at different temperature for 1 h. Overall, the surfaces of the three tempering temperatures all show a uniform distribution of ductile dimples. Microvoids can be clearly recognized under high magnifications. It can be deduced that the fracture mechanism of tempered martensite follows a more ductile mode compared to as-quenched martensite, showing that tempering process changed martensite from a brittle and hard microstructure to a more ductile microstructure, which coincides with the decreasing strength and increasing elongation with increasing tempering temperature.

The fracture surface of 250℃ and 400℃ are quite similar. For martensite tempered at 500℃, small cleavage facets containing river patterns are observed, separated by tear ridges (indicated by arrows in (e-f)), showing a likely typical quasi-cleavage fracture [35]. This kind of fracture usually occurs in the quenched and tempered specimen at relatively low temperatures, but in this case, due to the retarding effect of silicon, this temperature is elevated. However, most of the microstructures are still occupied with dimples and microvoids, indicating that the fracture mode of martensite tempered at 500℃ can be ductile mode or a mixed mode of ductile and quasi-cleavage.

4.3 Tempering of Bainitic Microstructures

4.3.1 Bainitic Microstructures

Microstructure characterization

Figure 4.8 shows the optical and scanning electron micrographs of bainitic microstructures obtained from isothermal treatment.

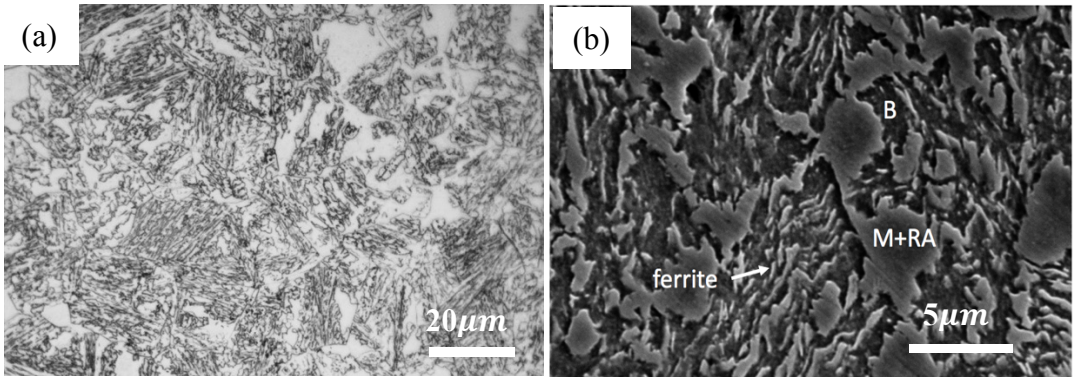

Figure 4.8: *Bainitic microstructure through isothermal treatment of 400℃ for 0.5 h and water quenching. (a) Optical micrograph (b) SEM micrograph. 2% Nital etched.*

Bainitic microstructure was formed by isothermal treatment of 400℃ for 0.5 h and water quenching to room temperature after austenization. The microstructure results are shown in Figure 4.8. After isothermal treating at 400 ℃ for 0.5 h, the cementite precipitation from austenite is suppressed at large concentrations of silicon, leading to the possibility to obtain a carbide-free distinctive microstructure. The fine plates of bainitic ferrite sheaves are separated by coarse block of retained austenite, which is shown in Figure 4.8 (b) [36, 37]. According to the CCT curve and the calculated cooling rate, some martensite is also formed in the microstructure which is transformed from the insufficient carbon-enriched residual austenite during the final quenching of bainitic transformation. No obvious carbide precipitation is observed, with most carbide precipitates exist on the lath boundaries of MA block, which is hardly distinguished in the figure.

Mechanical properties

The mechanical properties of bainite were characterized by hardness test and tensile tests. The results are displayed in Table 4.3.

Table 4.3: *Mechanical properties of bainite.*

	Hardness/HV1	**YS/MPa**	**UTS/MPa**	**Elong./%**
Bainite	369±10	816±8	1318±4	10.6±0.8

The lower hardness and strength than the as-quenched martensite are due to the predominantly present bainite sheaves formed during isothermal treatment in the microstructure [38]. Lower strength and higher elongation indicated that bainite is a more ductile and soft phase than martensite.

Fractography

Figure 4.9 illustrates the SEM images of fracture surfaces of bainitic microstructures tempered for 1 h.

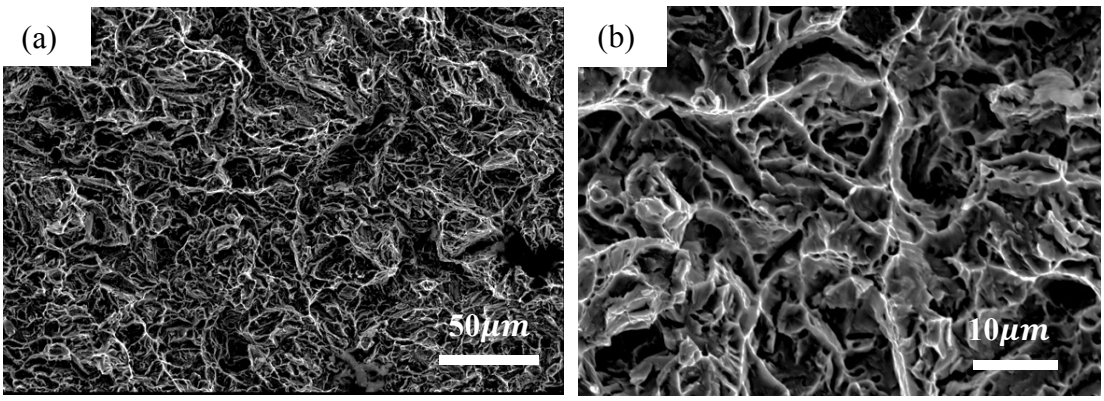

Figure 4.9: *SEM images of bainite fracture surface of different magnifications.*

The fracture of bainite is mainly determined by ferrite and the distribution of carbides. As shown in Figure 4.9, dimples and microvoids are homogeneously distributed among the whole microstructure, indicating that the fracture mode of bainite is ductile fracture. No cleavage planes can be seen from the microstructure, indicating that bainite is a more ductile and softer phase than as-quenched martensite, which can also be deduced from the lower strength and higher elongation value obtained from tensile tests. In addition, the bainite obtained is a carbide-free microstructure. The absence of brittle carbides also contributes to the difficulty in crack formation and void nucleation.

4.3.2 Effect of Tempering on Bainite

Microstructure characterization

Figure 4.10 and Figure 4.11 show the OM and SEM graphs of bainitic microstructures after tempering of different parameters, respectively.

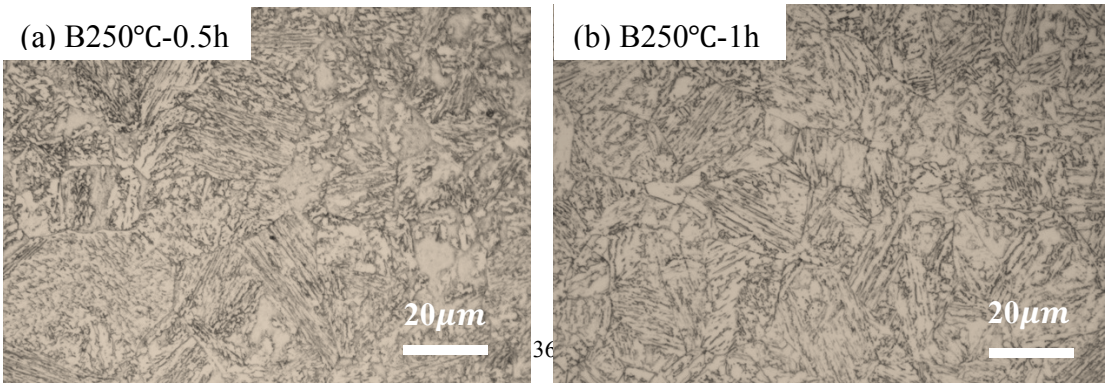

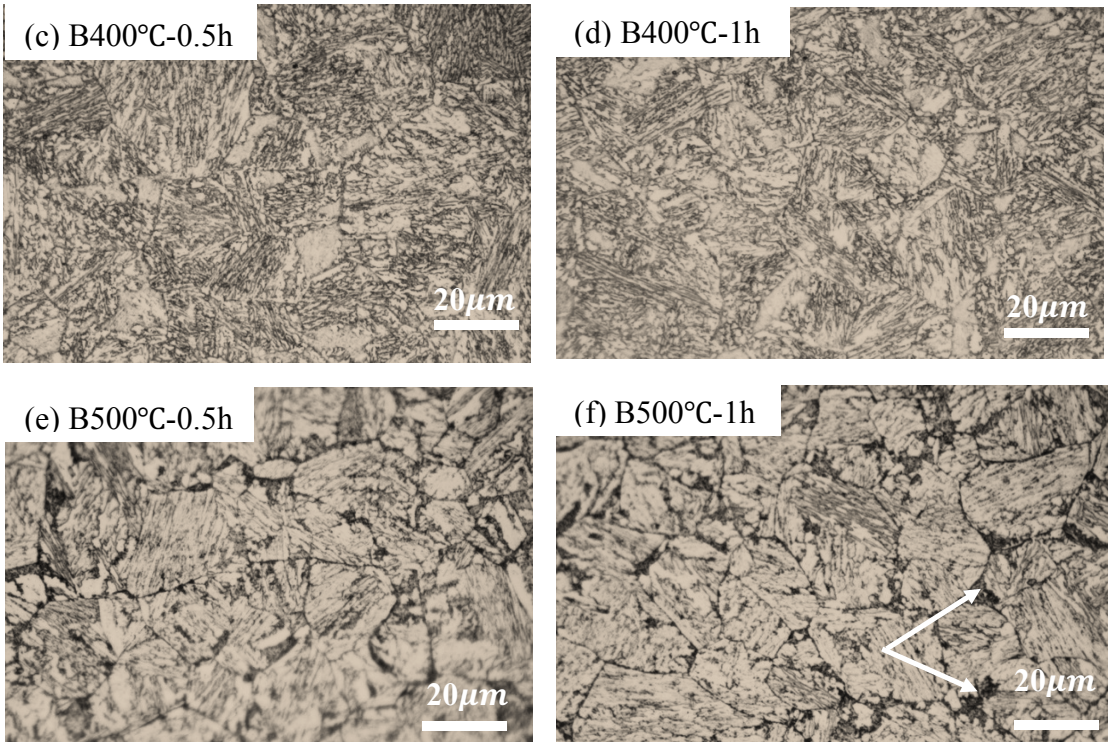

Figure 4.10: *Optical images of tempered bainite of different tempering temperatures and times. 2% Nital etched.*

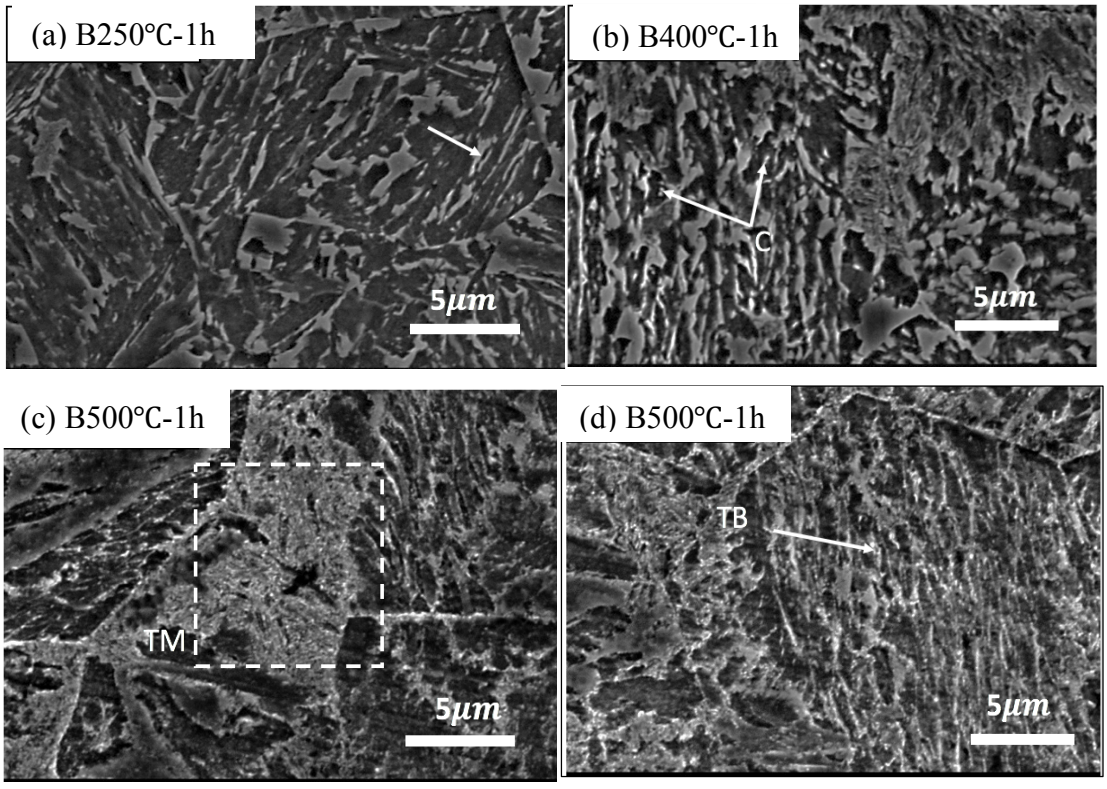

Figure 4.11: *SEM images of tempered bainite of different tempering temperatures for 1h. 2% Nital etched.*

For samples of the same tempering temperature but different tempering time, no perceptible change is observed.

As illustrated in Figure 4.10 and 4.11, clear grain boundaries can be distinguished for all three tempering temperatures. Similar to the tempering of martensite, the alloyed silicon in the microstructure retards the precipitation of cementite at 250℃ for that no clear precipitation is observed in Figure 4.10 (a-b). Bainite sheaves still remains in the microstructure, as shown by the arrow in Figure 4.11 (a). Decreasing blocky area with higher tempering temperature indicates the decomposition of martensite and retained austenite.

For the tempering at 400℃, small amount of carbide starts to precipitate due to the decomposition of carbon-enriched retained austenite, as shown in Figure 4.11 (b). No other perceptible change in the microstructure is observed from the untempered structure.

Since the microstructure before tempering is a mixture of bainite and martensite which was transformed from austenite during the final quenching, at tempering temperature of 500℃, tempered martensite and tempered bainite are both be observed in the microstructure, which are shown by the square region in Figure 4.11 (c) and (d), respectively. From Figure 4.10 (e-f), carbide precipitation occurs in tempered martensite along the lath and grain boundaries. While for tempered bainite, fine carbide precipitation occurred between the bainitic ferrite sheaves. The retained austenite decomposes to discrete carbide particles and ferrite. It can also decompose to pearlite [39], which cannot be confirmed through SEM.

Mechanical Properties

The mechanical properties of tempered bainite were characterized by hardness test and tensile tests. The results are displayed in Table 4.4. The influence of tempering treatments on yield strength, ultimate tensile strength, total elongation and room temperature hardness with varying tempering temperature and times were plotted in Figure 4.12 (a)-(d).

Table 4.4: *Mechanical properties of bainite after tempering.*

Sample	Hardness/HV1	YS/MPa	UTS/MPa	Elong./%
B250℃-0.5h	391 ± 9	886 ± 5	1294 ± 4	12 ± 0.1
B250℃-1h	389 ± 7	889 ± 5	1287 ± 8	11.9 ± 0.1
B400℃-0.5h	387 ± 7	986 ± 8	1228 ± 9	13.8 ± 0.1
B400℃-1h	386 ± 7	976 ± 6	1226 ± 3	14.4 ± 0.2
B500℃-0.5h	333 ± 4	872 ± 4	1046 ± 6	12 ± 0.8
B500℃-1h	332 ± 5	872 ± 3	1023 ± 2	11.8 ± 0.1

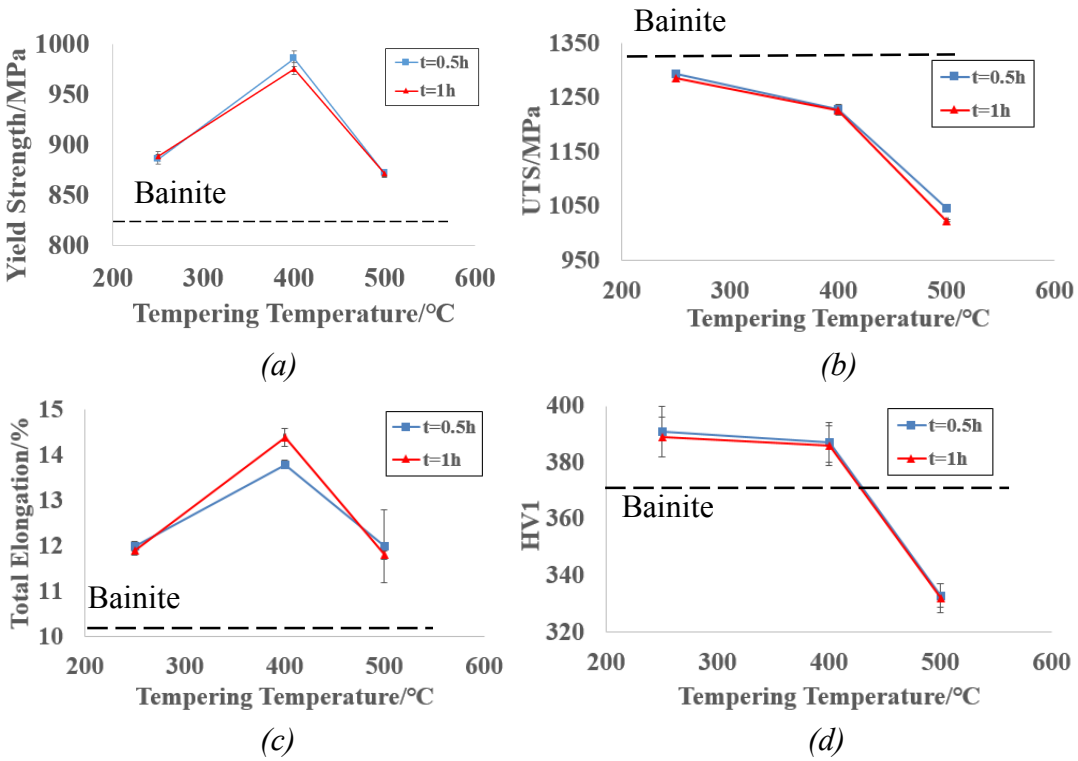

Figure 4.12: *Results of mechanical tests with tempering temperatures for bainite. The dashed line in each figure represents the value of untempered bainite.*

Overall, relatively low yield-tensile ratio can be obtained due to certain amount of retained austenite. This content was not measured in this work due to the limitation of time, therefore, further experiments of EBSD and XRD can be done to measure the content of retained austenite.

Retained austenite can lead to TRIP effect in the tensile tests of bainite, leading to the increased strength and elongation before 400℃, which is illustrated in Figure 4.12 (a) and (c). More retained austenite content in bainite also indicate higher carbon content in bainite than martensite. During tempering lower than 400℃, significant amount of supersaturated carbon precipitates in the microstructure, contributed both by the precipitation from bainitic ferrite and the decomposition of MA constituent. The fine carbides resist the motion of dislocations, leading to precipitation strengthening. The matrix is therefore strengthened, exceeding the softening effect due to the recovery of dislocations.

At 400℃, The MA constituent became finer and the space between them was also smaller, which increased the interface of martensite and ferrite and the strengthening effect during the formation of martensite.

At 500℃, the carbides grow and the strengthening effect decreases. The softening effect of retained austenite decomposition surpass the strength provided by precipitation, leading to a decrease in the yield strength. As for the tensile strength and the hardness, the tendencies are the same with those of tempered martensite, which were explained by the similar reasons in the previous contents. The elongation of bainite is considered to continuously increase with higher tempering temperature, due to the combined effect of the growth of carbides, the recrystallization of ferrite and the TRIP effect of the retained austenite. However, in this work, the elongation during tempering firstly increases and then decreases at 500℃ for both 0.5 h and 1h, which may be caused by unknown mechanisms which cannot be explained by the results from this project. Therefore, related experiments are recommended to study the reason of the decreased elongation at 500℃ tempering.

Fractography

The fracture surfaces after tensile tests were characterized by SEM and the results were shown in Figure 4.13 (a-f).

B250℃-*1h*

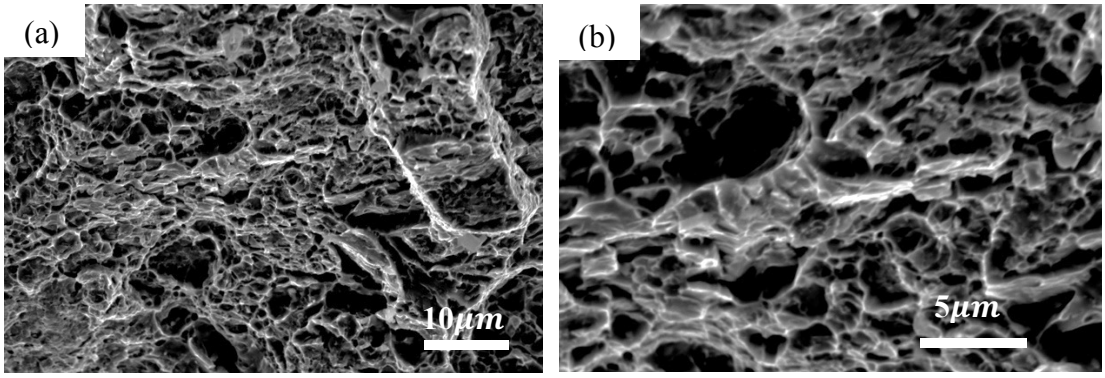

B400℃-*1h*

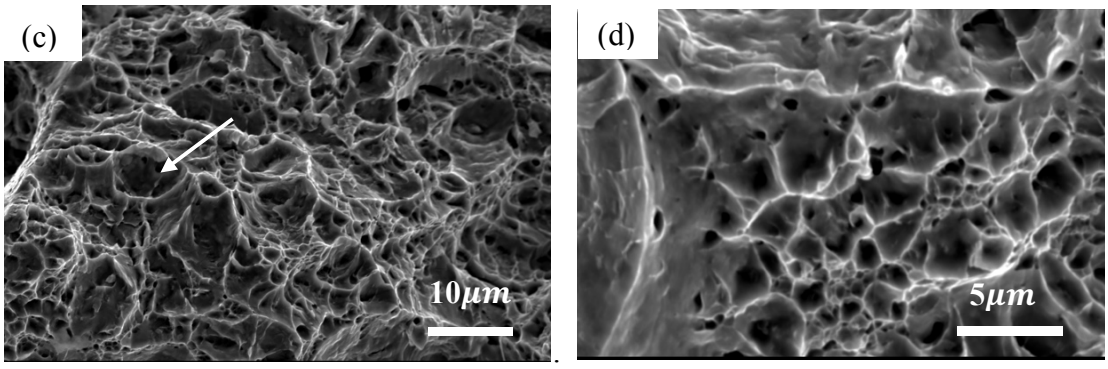

B500℃-1h

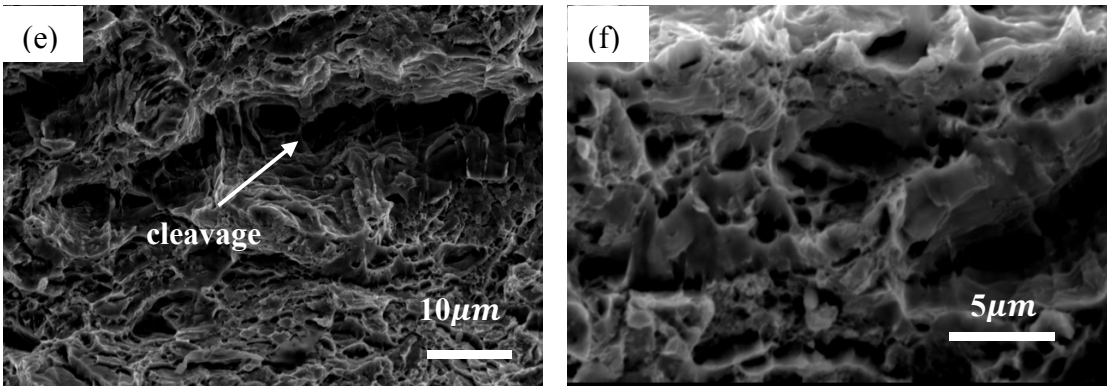

Figure 4.13: *SEM images of the fracture surfaces of bainite tempered for 1 h.*

The influence of isothermal time for 0.5 h and 1 h on the microstructure and properties of martensite and bainite cannot be deduced from above results. Experiments of longer tempering time and larger intervals between two times are recommended in order to study the effect of tempering time on martensite and bainite.

For bainite tempered at all three tempering temperatures, the microstructure of the fracture surface contains certain amount of dimples and also small cleavage facets containing river patterns, separated by tear ridges, showing a typical quasi-cleavage fracture [40].

Figure 4.12 (c-d) show that for samples tempered at 400℃, more dimples with larger size are observed, indicating at this temperature, the fracture mode is closed to ductile fracture, which can be proved by the high elongation and strength obtained from tensile tests.

(e-f) show that for samples tempered at 500℃, more cleavage places and tear ridges are observed than lower temperature. There is large amount of carbide precipitates in the bainitic microstructure which distributed discretely in the ferrite matrix. These coarsening carbide precipitates decrease the tensile strength and contributed to the brittleness at 500℃.

4.4 Comparison of Martensite and Bainite during Tempering

The comparison of microstructure and mechanical properties changes during tempering of martensitic and bainitic microstructures is summarized in this section. The detailed interpretations of the similarities and differences are also included.

Effect of silicon

Based on literatures, in tempering of both martensite and bainite, silicon retards the cementite precipitation at 250℃ tempering for martensite and bainite, only transitional carbides (most likely ε-carbide) occur.

Changes of mechanical properties before and after tempering

Compared to as-quenched martensite, tempering leads to a decrease in strength and hardness. Elongation is increased for tempered martensite. These changes in mechanical properties are resulted from the combination effects of carbides precipitation, recovery of dislocations and recrystallization of ferrite during tempering. Most carbon in as-quenched martensite is in solid solution and strengthens the microstructure by solid solution strengthening. During tempering, large amount of solid solute carbon form precipitates and the strengthening effect of solid solutes is strongly reduced.

Compared to bainitic microstructures before tempering, UTS decreases and elongation increases after tempering, which is similar to that of martensite. While the yield strength and hardness are higher than the untempered bainite. This is because that at tempering up to 400 ℃, transitional carbide precipitation takes place in bainite, leading to precipitation strengthening. Since almost all the carbon in bainitic microstructure is in the form of precipitates, this strengthening affects stronger in bainite than martensite.

Changes of mechanical properties with tempering

The comparative graphs of mechanical properties changes during the tempering of martensite and bainite are shown in Figure 4.14.

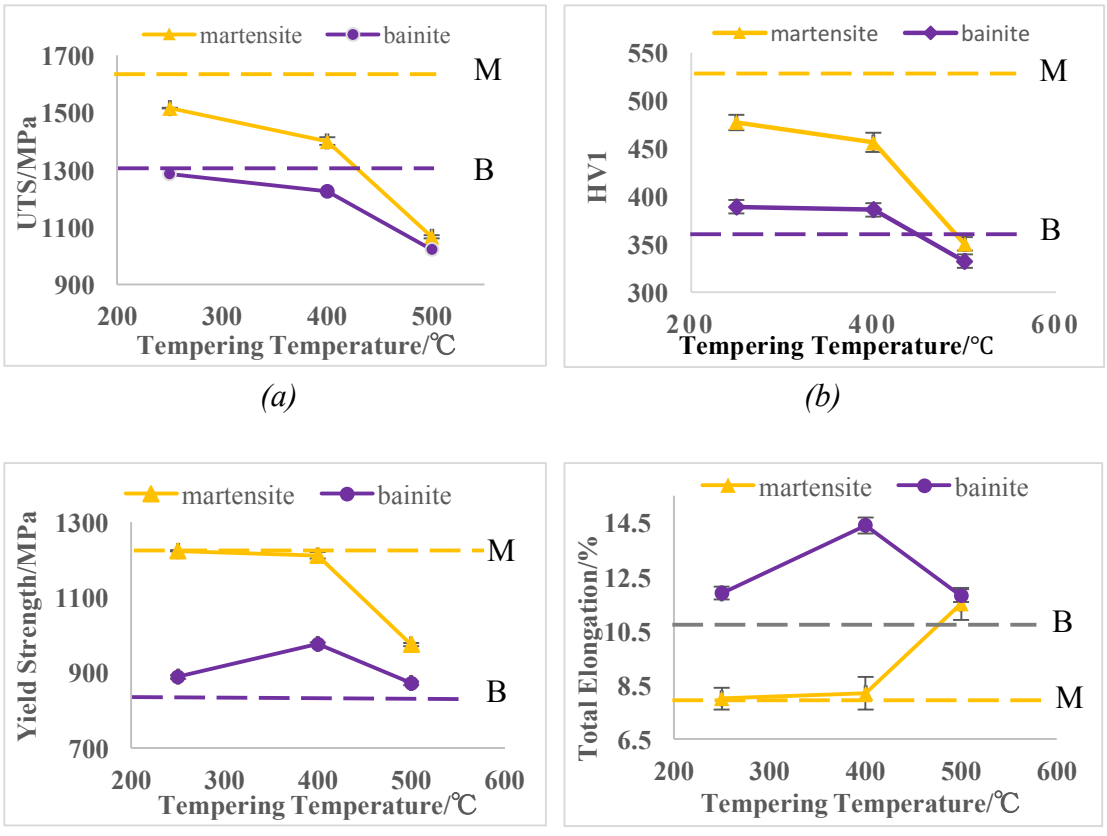

Figure 4.14: Comparison of mechanical properties change during the tempering of martensite and bainite. M-as-quenched martensite, B-bainitic microstructures.

From Figure 4.14 (a) and (b), it can be observed that for both martensitic and bainitic microstructures, tensile strength and hardness decrease with higher tempering temperatures. Tempering leads to significantly decreased strength and hardness as well as increased elongation of martensite. While bainite is not sensitive to tempering compared to martensite, for that its UTS and hardness are not strongly influenced by the tempering process.

(c) shows that the yield strength of martensite during tempering firstly remains the same due to the combined effect of precipitation strengthening and dislocation recovery. Then yield strength significantly decreases with the growth of precipitates and recrystallization. While for bainite, it firstly increases at tempering up to 400℃ due to the TRIP effect during tensile tests. With higher tempering temperature, yield strength decreases due to further recovery and recrystallization, which shares a similar mechanism with that of martensite.

In (d), the elongation of martensite continuously increases with higher tempering temperature. While for bainite, it firstly increases due to the certain amount of retained austenite in the microstructure. Then it decreases due to the recovery and recrystallization.

Fractography

As-quenched martensite is more brittle and hard than bainitic microstructure formed during isothermal treatment. The fracture mode of martensite tempered at 250, 400 and 500℃ shows ductile fracture, presenting with large amount of dimples and microvoids. Bainite tempered at all temperatures show a microstructure with cleavage and tear edges, indicating a quasi-cleavage fracture mode.

5 Conclusions

In this project, the influence of tempering on the microstructure & properties of martensite and bainite in a steel with composition Fe-0.2C-2Si-3Mn (wt.%) were studied. Tempering treatments were performed to martensitic and bainitic microstructure followed by mechanical tests. The fracture characterization of the fracture surfaces after tensile tests were also investigated. Conclusions drawn from the results and discussions above can be divided into three major respects.

Regarding Tempering of Martensitic Microstructures

- During the tempering of martensite, transitional carbide precipitation occurs instead of cementite at 250℃ due to the stabilization effect of silicon on transition carbides (ε-carbides). Most of carbides form along the grain boundary of prior austenite grain.
- The yield strength of martensite remains the same before 400 ℃ under the combined effect of the softening by decreasing dislocation density and the strengthening by carbide precipitation. After 400℃, the yield strength significantly decreases due to the recovery of dislocations and recrystallization of ferrite.
- The recovery of dislocations during the whole tempering process causes continuously decreased UTS and hardness, and an increase in total elongation.
- The fracture modes of tempered martensite for 250 and 400℃ show a typical ductile fracture with large quantity of dimples and microviods. For martensite tempered at 500℃, some cleavages occur showing a likely quasi-cleavage fracture mode, but dimples and voids still occupy the majority area of the microstructures.

Regarding Tempering of Bainitic Microstructures

- TRIP effect provided by retained austenite leads to enhanced yield strength and elongation before 400℃ tempering. The strength is also increased by fine carbide precipitates. When the temperature increases, the elongation continues to increase while the yield strength decrease with recovery and recrystallization.
- The hardness and UTS follow the same trend as in martensite, which continuously increase during tempering.
- Generally, the fracture surfaces for bainitic microstructures tempered at all temperatures show a quasi-cleavage fracture mode, demonstrated by cleavage facets containing river patterns and tear ridges. When tempering at 400℃, some large dimples are observed due to the increase in elongation, indicating a mixed mode of likely ductile and quasi-cleavage fracture. At 500℃, more cleavages and tears occur in the microstructure.

Regarding Comparative Response to Tempering

- Higher yield-tensile ratio is obtained in bainite than martensite, due to that large amount of retained austenite remains after isothermal treatments. Retained austenite contributes to higher strength and elongation during tempering.
- Bainite is less sensitive to tempering compared to martensite, because there are already carbides before tempering while most carbon in martensite is in solid solution. During tempering, large amount of carbide precipitations take place in martensite, leading to significant decrease in strength and hardness.

6 Recommendations

There are still some questions remaining that cannot be fully explained by the results obtained from this project. Therefore, recommendations of further researches are made in this section:

- Due to the fact that there is certain amount of retained austenite in the bainitic microstructures, higher strength and elongation were obtained through TRIP effect at 400℃ tempering than martensite, which contains almost no retained austenite. EBSD/XRD is recommended to measure the fraction of retained austenite in banite in order to study the explicit influence of retained austenite the mechanical properties during tempering.
- At 250℃ tempering of martensite and bainite, ε-carbides were expected to precipitate instead of cementite due to the high content of silicon, but the type of carbides cannot be determined by the results obtained from this project. Therefore, TEM is recommended for martensite and bainite tempered at 250℃ to examine whether the carbides are ε-carbides or other types of carbides.
- For B500℃-0.5h and B500℃-1h samples, the elongation showed a decrease, which was expected to increase continuously during tempering. This cannot be explained by the results obtained in the project. Therefore, repeated experiments are recommended to perform, in order to study the reason of this discrepancy.
- In this work, only 0.5 h and 1 h were chosen for each tempering temperature, and the results didn't show much difference in microstructures and properties between samples of these two tempering times. Therefore, experiments on samples of different tempering times and intervals are recommended in the further research.

Reference

[1] Krauss, G. Steels: processing, structure, and performance. Asm International, 2015.
[2] Bhadeshia, H. K. D. H. Bainite in Steels: transformations, microstructure and properties (Book; 735). IOM Communications, 2001.
[3] Speer, J., et al. Carbon partitioning into austenite after martensite transformation. Acta materialia, 2003, 51.9: 2611-2622.
[4] Bhadeshia, H. K. D. H.; Edmonds, D. V. Bainite in silicon steels: new composition–property approach. Metal Science, 1983, 17.9: 411-425
[5] Bhadeshia, H. Interpretation of the microstructure of Steels. Graduate Institute of Ferrous Technology, Web, 2010.
[6] Bhadeshia, H. Steels: microstructure and properties. Butterworth-Heinemann, 2006.
[7] Olson, G.; Owen, W. Martensite: a tribute to Morris Cohen. Asm International, 1992.
[8] Durand-Charre, M. Microstructure of steels and cast irons. Springer Science & Business Media, 2004.
[9] Chang, L. Bainite transformation temperatures in high-silicon steels. Metallurgical and Materials Transactions A, 1999, 30.4: 909-916.
[10] Mehl, R. Hardenability of alloy steels. ASM, Metals Park, 1939.
[11] Porter, David A.; Easterling, K.; Sherif, M. Phase Transformations in Metals and Alloys, (Revised Reprint). CRC press, 2009.
[12] Sawley, K. & Sun, J. Advanced rail steels: investigating the bainitic option. Railway Track & Structures, 1997, 3, 22-27.
[13] Morito, S. The morphology and crystallography of lath martensite in Fe-C alloys. Acta Materialia, 2003, 51.6: 1789-1799.
[14] Du, C. Block and sub-block boundary strengthening in lath martensite. Scripta Materialia, 2016, 116: 117-121.
[15] Berns, H. Ferrous materials: steel and cast iron. Springer Science & Business Media, 2008.
[16] Navarro-López, A., et al. Characterization of bainitic/martensitic structures formed in isothermal treatments below the Ms temperature. Materials Characterization, 2017, 128: 248-256
[17] Hell, J., et al. Microstructure–properties relationships in carbide-free bainitic steels. ISIJ international, 2011, 51.10: 1724-1732.
[18] Rao, B. Structure-property relations and the design of Fe-4Cr-C base structural steels for high strength and toughness. Metallurgical and Materials Transactions A, 1980, 11.3: 441-457.
[19] Argon, A. Strengthening mechanisms in crystal plasticity. Oxford University Press on Demand, 2008.
[20] Taylor, G. The mechanism of plastic deformation of crystals. Part I. Theoretical. Proceedings of the Royal Society of London. Series A, Containing Papers of a Mathematical and Physical Character, 1934.

[21] Gottstein, G. Physical foundations of materials science. Springer Science & Business Media, 2013.
[22] Gladman, T. The physical metallurgy of microalloyed steels. Maney Pub, 1997.
[23] Dieter, G. Mechanical metallurgy. New York: mcgraw-hill, 1986.
[24] Orowan, E. Discussion in The Symposium on Internal Stresses in Metals and Alloys, Inst. Metals, London, 1948, 451.
[25] Bhadeshia, H. The bainite transformation in a silicon steel. Metall Mater Trans A, 1979, 10: 895–907.
[26] Kang, J. Effect of tempering on the microstructure and mechanical properties of a Medium carbon bainitic steel. Materials Science & Engineering, 2017.
[27] Standard, A. S. T. M. E8/E8M. Standard test methods for tension testing of metallic materials. ASTM international, West Conshohocken PA, 2009.
[28] Van Bohemen, S. M. C.; Sietsma, J. Martensite formation in partially and fully austenitic plain carbon steels. Metallurgical and Materials Transactions A, 2009, 40.5: 1059-1068.
[29] Andrews, K.W. Empirical formulae for the calculation of some transformation temperatures. J. Iron Steel Inst, 1965, 203.7: 721-727.
[30] Gorni, A. Steel forming and heat treating handbook. São Vicente, Brazil, 2011, 24.
[31] Lee, Y. Empirical formula of isothermal bainite start temperature of steels. Journal of materials science letters, 2002, 21.16: 1253-1255.
[32] Mertz, J. Introduction to optical microscopy. Roberts, 2010.
[33] John, V. Testing of materials. Macmillan Publishers Limited, 1992.
[34] Hu, Y. Phase transformations in steels during quenching and partitioning heat treatment, 2016. Thesis TU Delft.
[35] Liu, A. Mechanics and mechanisms of fracture: an introduction. ASM International, 2005.
[36] Liu, D. Effect of tempering temperature and carbide free bainite on the mechanical characteristics of a high strength low alloy steel. Materials Science and Engineering, 2004: A, 371(1), 40-44.
[37] Long, X. Carbide-free bainite in medium carbon steel. Materials & Design, 2014.
[38] Luzginova, N. Bainite formation kinetics in high carbon alloyed steel. Materials Science and Engineering: A, 2008, 481: 766-769.
[39] Garcia-Mateo, C., et al. Tempering of hard mixture of bainitic ferrite and austenite. Materials Science and Technology, 2004, 20.7: 814-818.
[40] De Cooman, B. C. Structure–properties relationship in TRIP steels containing carbide-free bainite. Current Opinion in Solid State and Materials Science, 2004, 8.3: 285-303.